NANYANG TECHNOLOGICAL UNIVERSITY
SINGAPORE

Polytetrafluoroethylene (PTFE) Hollow Fibre Membrane Fabrication for Organic Solvent Nanofiltration (OSN)

VERONA NITHYA FRANCIS
SCHOOL OF CIVIL AND ENVIRONMENTAL ENGINEERING

2022

Polytetrafluoroethylene (PTFE) Hollow Fibre Membrane Fabrication for Organic Solvent Nanofiltration (OSN)

VERONA NITHYA FRANCIS

School of Civil and Environmental Engineering

A thesis submitted to the Nanyang Technological University in partial fulfilment of the requirement for the degree of Master of Engineering

2022

Statement of Originality

I hereby certify that the work embodied in this thesis is the result of original research, is free of plagiarised materials, and has not been submitted for a higher degree to any other University or Institution.

21/07/2022

. . . . . .

Date

. . . . . .

Verona Nithya Francis

Supervisor Declaration Statement

I have reviewed the content and presentation style of this thesis and declare it is free of plagiarism and of sufficient grammatical clarity to be examined. To the best of my knowledge, the research and writing are those of the candidate except as acknowledged in the Author Attribution Statement. I confirm that the investigations were conducted in accord with the ethics policies and integrity standards of Nanyang Technological University and that the research data are presented honestly and without prejudice.

22/07/2022

. . . . . .

Date

. . . . . .

Wang Rong

Authorship Attribution Statement

This thesis **does not** contain any materials from papers published in peer-reviewed journals or from papers accepted at conferences in which I am listed as an author.

21/07/2022

. . . . . .

Date

. . . . . .

Verona Nithya Francis

Acknowledgements

I would like to take this opportunity to thank Nanyang Technological University for awarding me the NTU Research Scholarship to pursue my master's degree. I would also like to thank the Nanyang Environment and Water Research Institute and the Singapore Membrane Technology Centre for providing the facilities and funding for my research.

I would like to extend my gratitude to my main supervisor, Professor Wang Rong, for giving me this opportunity and for all the support and advice she has given me. I would like to thank Dr. Chong Jeng Yi for his guidance throughout my research journey and for his reassurance during experimental failures. I would also like to thank Professor Atsushi Goto, for kindling my interest in research during my undergraduate studies.

I would like to thank my friends, new and old, for their unwavering support and words of encouragement during my two years of research. Finally, I would like to thank my family, for being my pillar of support and for shaping me to be the researcher I am today.

Table of contents

Abstract

Membrane technology has allowed purification to be done in a cheaper and more energy efficient way. In organic solvent nanofiltration (OSN), material choice is important as the membrane must be able to withstand harsh solvents over a long time. Although polytetrafuoroethylene (PTFE) is known to be an inert material, little research has been done on using it for OSN membranes, due to fabrication challenges. In this study, the author has successfully synthesized PTFE hollow fibre thin film composites for OSN, despite challenges in the surface morphology and substrate hydrophilicity. The resultant membranes showed to have excellent chemical and mechanical stability when tested in harsh aprotic solvents such as dimethylformamide (DMF) and dimethylsulfoxide (DMSO). They showed high DMF permeance of 3.70 $lm^{-2}h^{-1}bar^{-1}$, and high acid fuchsin dye rejections of >90%. The membranes were also stable at pressures of up to 5 bar, and overtime.

List of Tables

List of Figures

Abbreviations

API	Active Pharmaceutical Ingredient
PTFE	Polytetrafluoroethylene
PVDF	Poly(vinylidene fluoride)
OSN	Organic Solvent Nanofiltration
TFC	Thin Film Composite
IP	Interfacial Polymerization
PES	Polyether sulfone
PDA	Polydopamine
PEI	Poly ethyleneimine
PIP	Piperazine
MPD	m-Phenylenediamine
TMC	Trimesoyl chloride
SDS	Sodiumdodecyl sulfate
RB	Rose Bengal
AF	Acid Fuchsin
MO	Methyl Orange
SO	Sudan Orange
SWCNT	Single Wall Carbon Nano Tube
MWCNT	Multi Wall Carbon Nano Tube
CHN	Copper Hydroxide Nanostrand
EDA	Ethylene Diamine
PEG	Polyethylene Glycol
MWCO	Molecular Weight Cut Off
GPC	Gel Permeation Chromatography
SEM	Scanning Electron Microscopy

FTIR	Fourier Transformed Infrared Microscopy
MOF	Metal Organic Framework
TA	Tannic Acid
MWCO	Molecular Weight Cut-Off

1 Introduction

Membrane separation is an emerging technology that has gained popularity since the 1960s [1]. It is a physical separation process whereby the feed solution is introduced on one side of the membrane and the permeate is collected on the other. These membranes have 'pores' that only allow certain molecules to pass through them, retaining the larger molecules on the opposite side. For nanofiltration, the word pore does not refer to physical pores in the membranes but rather, refers to the free volume within the polymer matrix [2]. Different membranes have different pore sizes, allowing them to have a variety of uses. Most of the time, membranes require a driving force such as pressure or voltage to enable the feed to permeate through the membrane. The various types of membranes and their pore size ranges are illustrated in Figure 1.

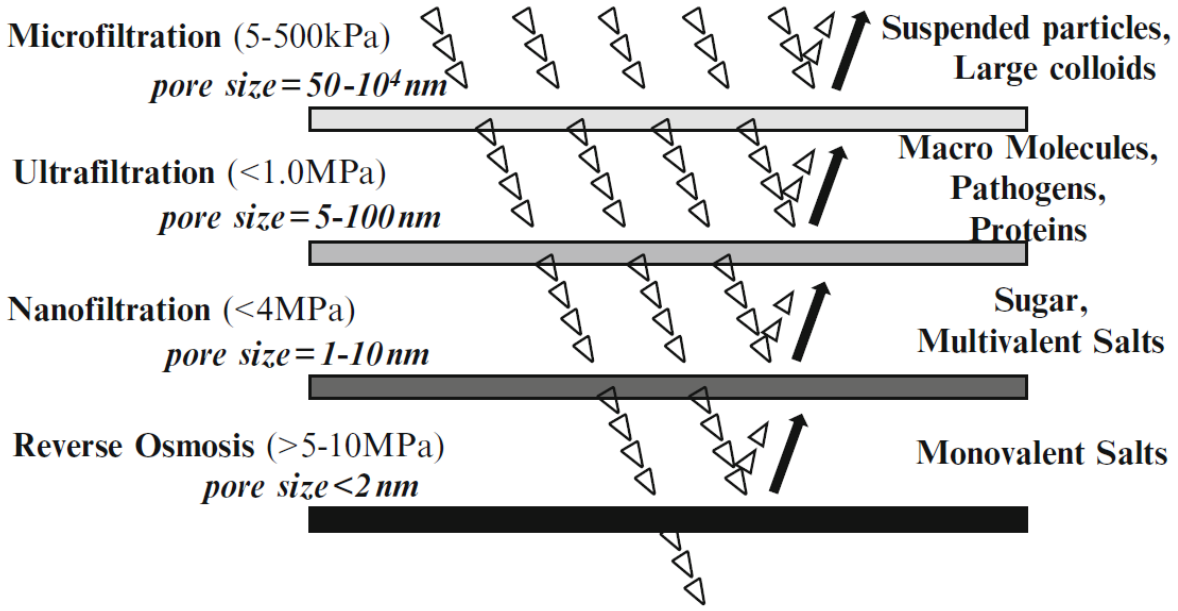

Figure 1 Types of pressure driven membranes [1]

Membranes have since become widely used, especially in the pharmaceutical industry, that has been growing at an exponential rate [3]. Their operations include the preparation and purification of Active Pharmaceutical Ingredients (APIs), which is done through several steps. In each of these steps, various solvents, including water, are used as a reaction medium. To reduce wastage, the used solvents are purified and reused for subsequent reactions [4]. As such, the pharmaceutical industry heavily relies on the science behind chemical separation and purification.

Existing purification technologies include distillation, crystallization, solvent extraction and chromatography [5]. These processes are necessary to remove trace amounts of impurities that could be hazardous or affect drug efficacy, all of which require the use of solvents. Apart from API purification, solvent recovery can offer significant benefits with regards to reduced purchase, storage, and waste costs [6]. Solvents are conventionally purified through either distillation or evaporation, before being reused. There are some drawbacks to using these conventional technologies. For example, distillation requires much energy for the phase transformation from liquid to gas and chromatography is not suitable for large scale operations [7]. These separation methods are generally costly, energy intensive and unsustainable, making developments in this field attractive.

The growing need for cheaper, energy-efficient purification has led to a greater interest in membrane technology, especially within the fast-growing pharmaceutical industry. Membrane purification is known to be more energy efficient than conventional purification technologies [8]. It is essential that the membranes used are chemically resistant and give products of high purity.

Organic Solvent Nanofiltration (OSN), or solvent resistant nanofiltration, can be employed, allowing separations of organic mixtures down to the molecular level. These membranes can, for example, be used in drug synthesis between steps or in downstream processing, minimising solvent waste, costs, and energy consumption [6]. Nanofiltration membranes have a molecular weight cut off (MWCO) between 200 and 1000Da [1], and is even able to reject multivalent ions, meeting the high purity criteria required in pharmaceuticals [4, 5].

Membrane separation has its own set of challenges. One general challenge is that there is a trade-off between permeability and rejection [9, 10]. A membrane with better rejection will inevitably have a lower flux due to the smaller pore size [11]. Another challenge is that there are not many large scale OSN processes in place despite the numerous pilot-scale tests that are ongoing. This is due to a lack of solvent resistance of the membranes in a wide range of solvents over a long time [12]. Some common polymeric materials that are used as the support structures for thin film composites

(TFCs) include polysulfone (PSF), polyether sulfone (PES) and poly(vinylidene fluoride) (PVDF) [12, 13]. These materials have low resistance to strong solvents like DMSO and DMF and thus, are not the best material choice for OSN applications. Other challenges include ensuring good membrane selectivity, swelling of the polymer and ensuring enough capital investment for industries to install new nanofiltration plants [14].

Polytetrafluoroethylene (PTFE) has high chemical and thermal resistance, making it an attractive membrane material for OSN. However, due to its inert nature, PTFE membrane preparation is limited to sintering, spinning and pore forming agent methods [15]. These methods result in a porous membrane structure, making it useful for applications such as membrane distillation [16] and microfiltration, but not as useful for nanofiltration and osmosis. To make PTFE membranes with rejection in the nanofiltration range, fabrication is required.

Potential challenges of the fabrication include ensuring the polyamide layer is thin and even and getting the polyamide layer to be formed close to the substrate surface. This is a challenge as PTFE membranes formed by the above-mentioned processes do not have a uniform pore size. It is also difficult for the polyamide layer to be formed on the substrate as the membrane must be sufficiently saturated with the aqueous phase despite the hydrophobic nature of PTFE. Having the layer close to the substrate will aid in the membrane's long-term stability and reduce the amount of swelling in solvents.

In this study, the author aims to synthesize an inert and robust hollow fibre thin film composite membrane by harnessing the chemical stability of PTFE and overcome the challenges of the substrate's large and uneven pore size and its high surface hydrophobicity. Through this, the author aims to investigate:

i. The OSN membrane performance in DMF
ii. The effect of monomer concentration and molecular weight on membrane performance
iii. The effect of additives on the MWCO of the membranes
iv. The chemical stability and performance of the membranes across various strong aprotic solvents
v. The stability of the membranes overtime and at high pressures

2 Literature review

2.1 Hollow fibres and Flat sheets

The two most common membrane types are flat sheets and hollow fibers [17]. Flat sheet membranes are the traditional membranes, where the liquid to be filtered (feed) is passed through a paper like membrane on one side and the permeate is collected on the other. This is known as a dead-end filtration mode where the feed flows perpendicular to the membrane surface and the permeate collected on the opposite side. The disadvantage of this mode is that fouling occurs easily, reducing the permeability and potentially clogging the membrane overtime. As such, regular cleaning is required.

Hollow fiber membranes have a 'tube-like' shape. These membranes have a small diameter of only 50-100 microns and several individual fibers are packed together in a bundle to form a membrane module. Commercial hollow fiber modules are usually 1m in length and 0.2-0.25m in diameter, containing around 10^6 individual fibers [18]. Figure 2 shows the schematic of a single hollow fiber.

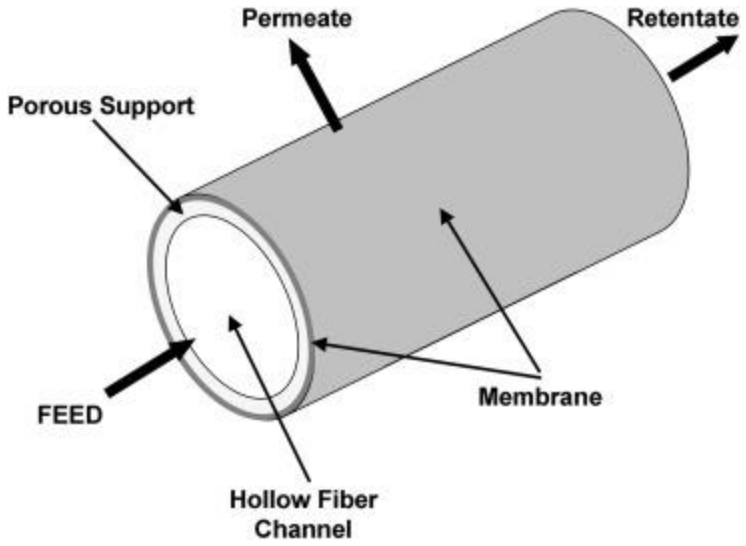

Figure 2 Schematic of a Hollow Fiber [19]

Instead of a dead-end mode, hollow fibers operate in a crossflow mode, where the feed flows in a direction perpendicular to that of the permeate. For an inside-out

configuration, the feed is pumped through the lumen and permeates radially through the membrane. The outside-in configuration is the opposite. The feed that does not permeate through is called the retentate and is recycled back into the feed. Such membranes have less fouling, higher packing density and is easier to scale up as compared to the flat sheet membranes [20]. Figure 3 illustrates the difference between crossflow and dead-end flow.

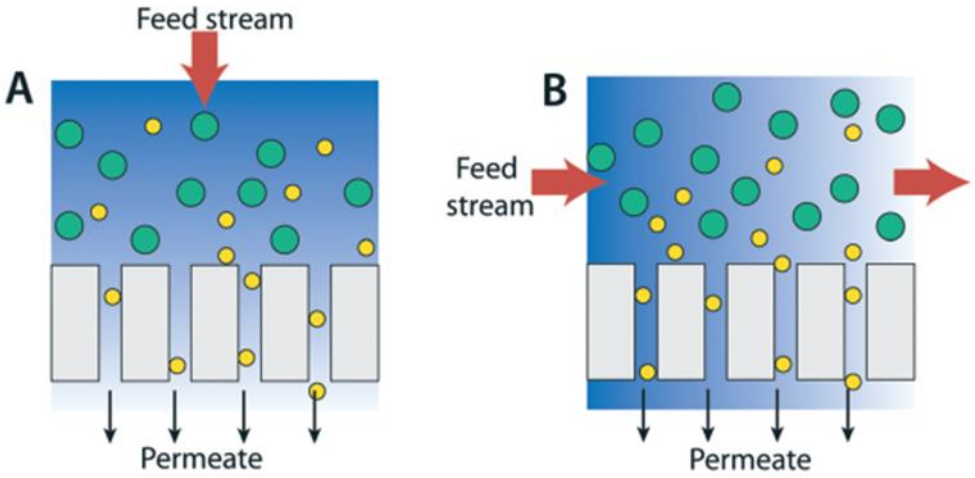

Figure 3 Crossflow versus Dead-end flow [21]

One way to synthesize polymeric hollow fibers is through the dry-jet or wet-jet spinning technique. This is where a polymer is first dissolved in a solvent and is then extruded through the spinneret. An illustration of this can be found in Figure 4 below. The polymer goes in the dope solution compartment while the bore fluid is one that is later remover to form the hollow fiber membrane.

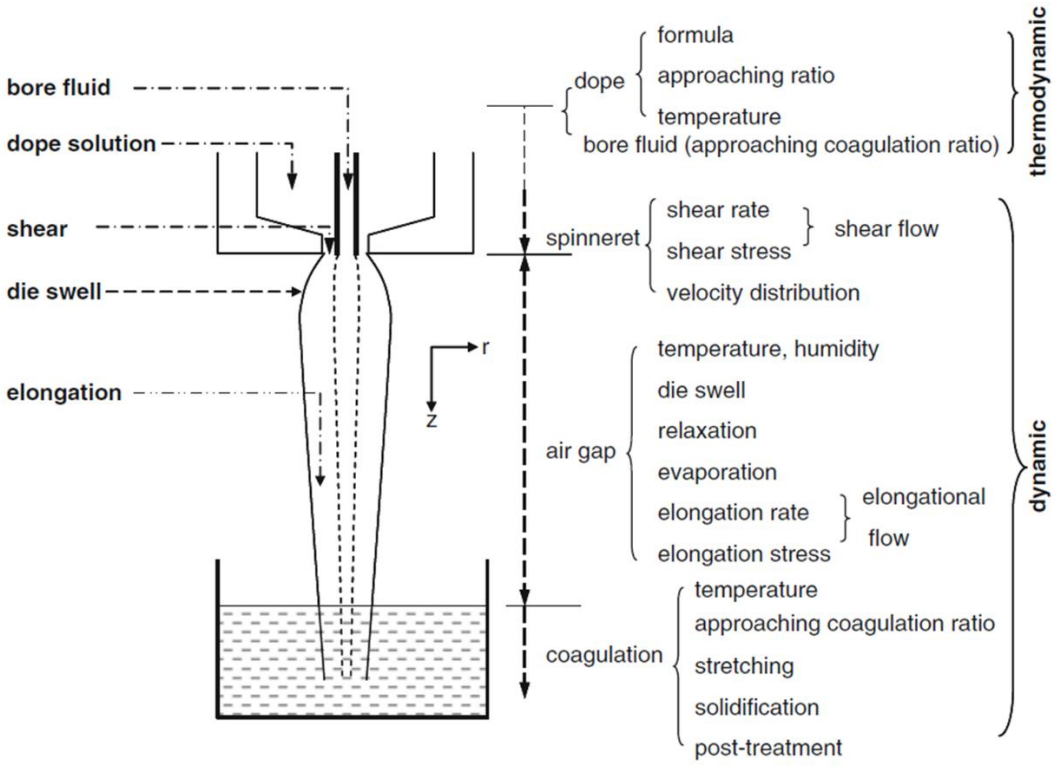

Figure 4 Illustration of a Spinneret [1]

Various factors affect the morphology of the resulting hollow fiber. Some of these are the shear rate, temperature of the coagulation bath and air gap height. This technique has been used to synthesize various polymeric substrates such as polyimide [22], PES [23] and even PVDF [24].

Both hollow fibres and flat sheets have been used in OSN. However, recent studies have focused on hollow fibres rather than flat sheets due to their advantages and scale-up capabilities. As such, the author has chosen to focus on the use of such hollow fibres in aims of their commercialization.

2.2 Thin Film Composites

Thin Film Composite (TFC) membranes are made of two or more polymeric materials consisting of a thin, dense barrier layer formed on top of one or more support layers [1]. The thin layer, around 0.1 microns thick, aids in reducing mass transfer resistance, resulting in a higher water flux. Figure 5 shows an illustration of the structure of a TFC membrane.

Figure 5 Thin Film Composite Membrane [21]

By incorporating the properties of two or more materials, it is possible to tailor the membranes to have high solvent stability, rejection, and flux. Typically, the thin dense top layer will provide for the rejection properties while the porous support layer provides for the overall mechanical properties of the membrane. Methods to form these membranes include dip coating and interfacial polymerization [14].

The choice of support material is important for OSN membranes as the support must be chemically inert to filter the harsh solvents in the feed solution [25]. Inorganic membrane supports such as ceramic hollow fibres have been previously used as they do not require any pre-treatment prior to IP [20]. This is due to their excellent chemical stability in a variety of organic solvents, and are even stable in DMF, a strong polar aprotic solvent [26, 27]. However, apart from being expensive, ceramic membranes are also difficult to scale up. Other than ceramics, polymeric supports have also been studied as they have the advantage of being lighter, cheaper, and easier to upscale. Table 1 shows a list of common materials used for membrane supports, the type of membrane (ultra or nanofiltration) as well as their monomer structure.

Table 1 Various Polymers for TFC Support Structure [14]

Polymer	Membrane type	Structure
Polyacrylonitrile (PAN)	NF, UF	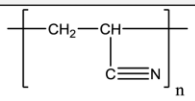
Polyimide (PI) Matrimid	NF, UF	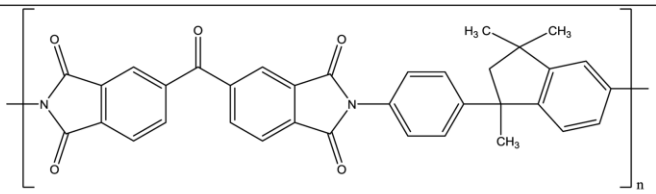
Polyimide (PI) P84	NF, UF	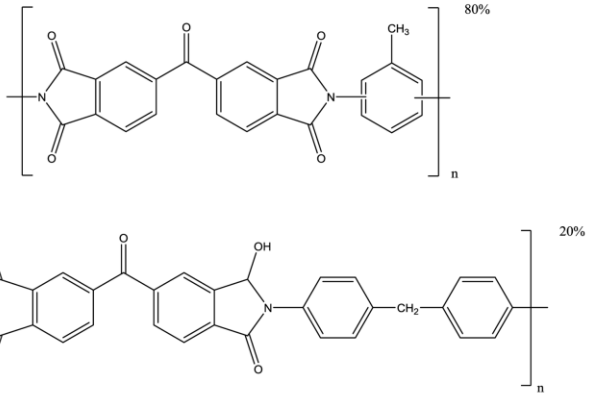
Polyaniline (PANI)	NF	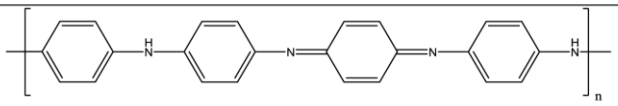
Polybenzimidazole (PBI)	NF	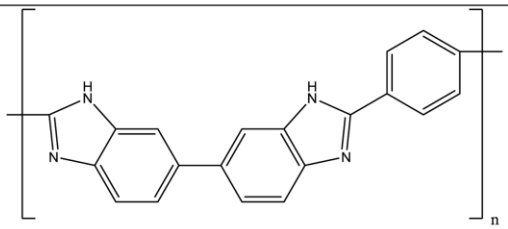
Polysulfone (PSf) + sulfonated poly (ether ether ketone) (SPEEK)	NF	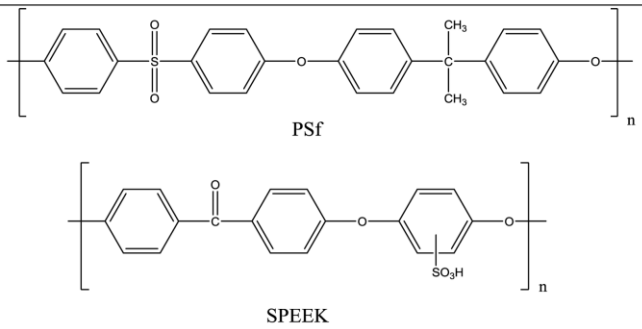
Poly (ether ether ketone) (PEEK)	UF	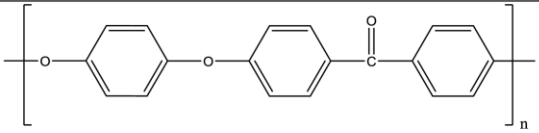
Polypropylene (PP)	UF	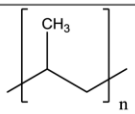

However, most polymeric materials, are not suitable for OSN due to their tendency to swell and their lack of chemical resistance [28]. Apart from increasing chemical resistance, crosslinking also increases the material's mechanical strength and reduces its swelling in solvents due to the restricted movements of the polymer chains within the polymer matrix [29]. Some studies also show that crosslinking can improve surface hydrophilicity [30]. One of such widely used chemically crosslinked materials for OSN would be polyimide, where several studies have suggested multiple ways of crosslinking the material which include UV crosslinking, thermal crosslinking, and chemical crosslinking [30, 31]. Although crosslinking does improve the membranes resistance, it in turn, however, reduces the membranes permeability, making it suboptimal for use [32]. As such there is a need for TFC membranes with chemically inert polymeric supports.

2.3 Interfacial polymerization

Interfacial polymerization (IP) is a polymerization reaction that occurs at the interface of two phases to form an ultra-thin functional layer on top of a chemically different porous support [14, 33]. Usually, one of the monomers will be soluble in the aqueous phase and the other in the organic phase. This is a simple and reliable process which is easy to scale up [34]. The IP process is illustrated in Figure 6 below.

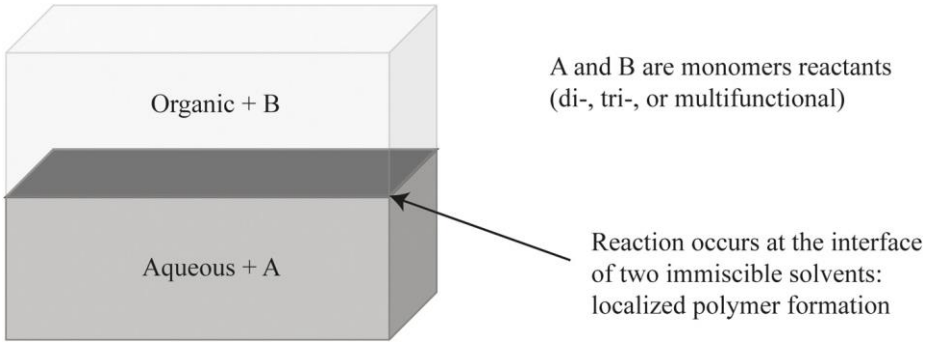

Figure 6 Organic and Aqueous phases in Interfacial Polymerization [33]

For TFC, the thin selective layer can be formed through interfacial polymerization and is usually made from polyamide. The porous supports are saturated in one of the phases, usually the aqueous phase, and later exposed to the other phase. The aqueous solution within the pores of the support will then diffuse into the organic phase, creating a thin selective polymeric barrier on the surface. There are many factors that

affect the IP process, such as monomer ratio, temperature, pH and presence of additives [35]. The surface morphology of the underlying substrate also plays a role in ensuring even IP. For instance, smaller substrate pores would result in a lower amount of aqueous phase being retained by the pores and hence, a thinner selective layer [36].

2.4 Top selective layer

Typically, polyamide is used as the top selective layer due to its high permeability, chemical stability, and ability to reject dissolved impurities [14, 37]. This polyamide layer is usually formed via the reaction between amine and acyl chloride monomers, forming the amide bonds. Since the amine monomers are soluble in aqueous medium, and acyl chlorides in organic medium, the two types of monomers can react together through a process called interfacial polymerization (IP), as discussed in section 2.3. There have been studies done where on top of using PEI, piperazine (PIP) is also added as a crosslinker to further control the MWCO of the synthesized membrane. A probable chemical structure from this reaction is illustrated in Figure 7.

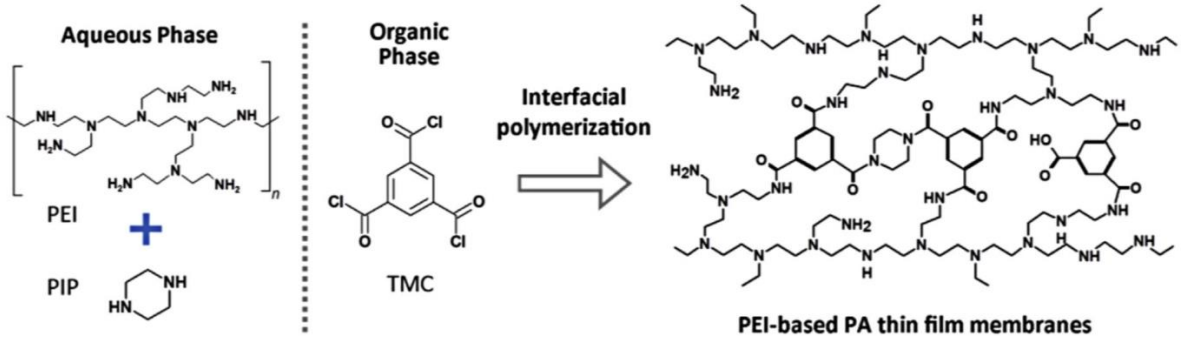

Figure 7 Possible reaction between PEI + PIP and TMC [20]

There have been a variety of monomers used to synthesize the selective polyamide layer. Most common amine monomers include polyethyleneimine (PEI) and m-phenylenediamine (MPD). MPD tends to be used more for reverse osmosis purposes due to its low MWCO from the tighter polyamide matrix [38]. PEI tends to form a looser polyamide matrix with a larger MWCO making it more useful for the separation of slightly smaller molecules. Piperazine (PIP) is sometimes added into the aqueous phase to increase crosslinking and form a tighter polyamide network. The most used acyl chloride used is trimesoyl chloride (TMC). TMC has three acyl chloride groups,

allowing for a higher crosslinking degree and a dense microstructure [25]. Choosing the right monomers and tailoring this polyamide layer is crucial as its thickness, surface morphology and crosslinking density will affect the membranes overall performance [39].

2.5 Substrate surface modification

Surface modification is done to impart desirable surface properties while retaining the desired bulk polymer properties such as chemical and mechanical strength [40]. Hydrophobic polymeric substrates need to be surface modified prior to IP to ensure the substrate pores are sufficiently saturated with the aqueous layer. Polytetrafluoroethylene (PTFE) is an example of such a material and one way to modify its surface is through plasma polymerization. In a study, PTFE samples were treated in plasma-based Ar beams and exposed to air to introduce -OH groups onto the surface. Contact angle measurements were taken the average water contact angle dropped from 102º to 86º [41]. Although the change may seem minimal, it is to be noted that improvements in hydrophilicity for PTFE is often limited [42]. An illustration of this process can be seen in Figure 8 below.

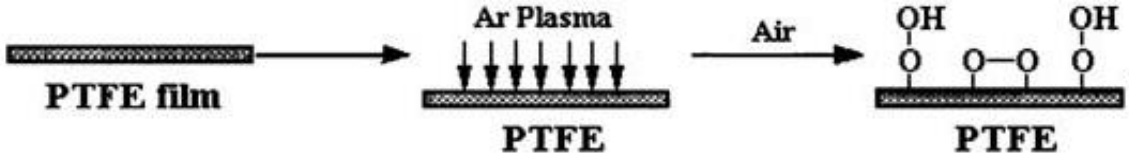

Figure 8 An illustration of plasma polymerization [41]

Although plasma polymerization can introduce new chemical functional groups and improve the hydrophilicity of PTFE, the process is tedious and complex. To make the process more feasible for commercialization, a simpler surface modification process is required.

A simpler way to modify the surface is by coating its surface with polydopamine (PDA). The idea for PDA as a surface adhesive came by studying mussels [43]. It was speculated that the coexistence of catechol and amine (lysine) groups may be crucial for achieving adhesion of mussels on almost any surface. Dopamine was found to

contain both these groups. The formed PDA layer is known to have strong adhesion to the membrane surface through covalent and hydrogen bonding [42]. $CuSO_4$ and H_2O_2 catalysts are often added to increase the PDA deposition rate [44]. Cu^{2+} and H_2O_2 produce reactive oxygen species that react with dopamine to form dopamine quinone. Subsequently, cyclisation occurs to form PDA. This process is illustrated in Figure 9 below.

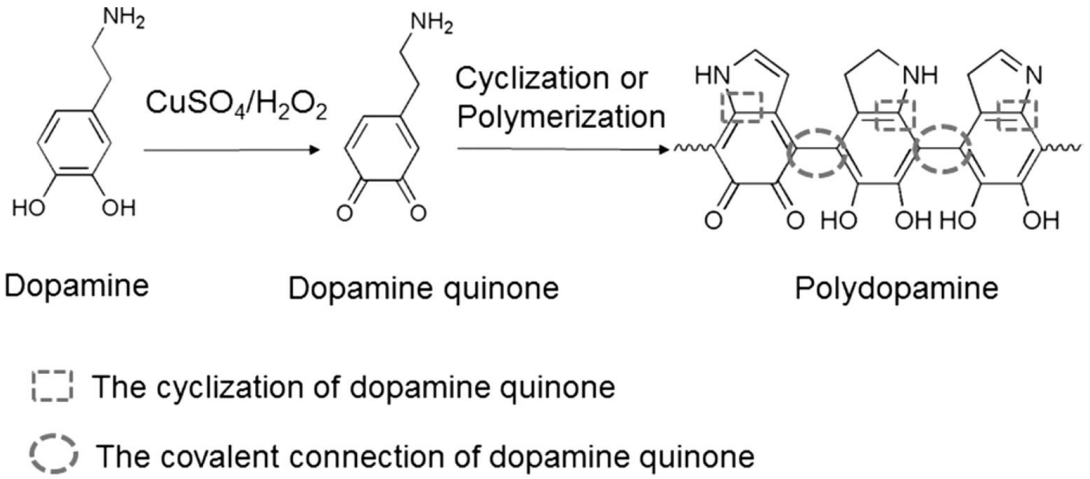

Figure 9 Dopamine Cyclisation [44]

A substrate color change from white to dark brown is an indication of PDA deposition. It was found that the addition of $CuSO_4$ and H_2O_2 caused this color change to occur within 30 to 40 mins as compared to several hours or days without the catalyst. This simple coating method is more practical and scalable for future commercialization as compared to other surface modification methods.

2.6 Interlayers

An interlayer is a layer than can be introduced prior to IP and sits between the porous support and thin selective layers. The interlayer can overcome the tradeoff between flux and rejection [9, 10] as well as provide a better surface for IP. It can also increases the amount of aqueous layer stored during soaking and help with an even selective layer formation [45]. Figure 10 below shows an overview on the type of interlayers in recent studies.

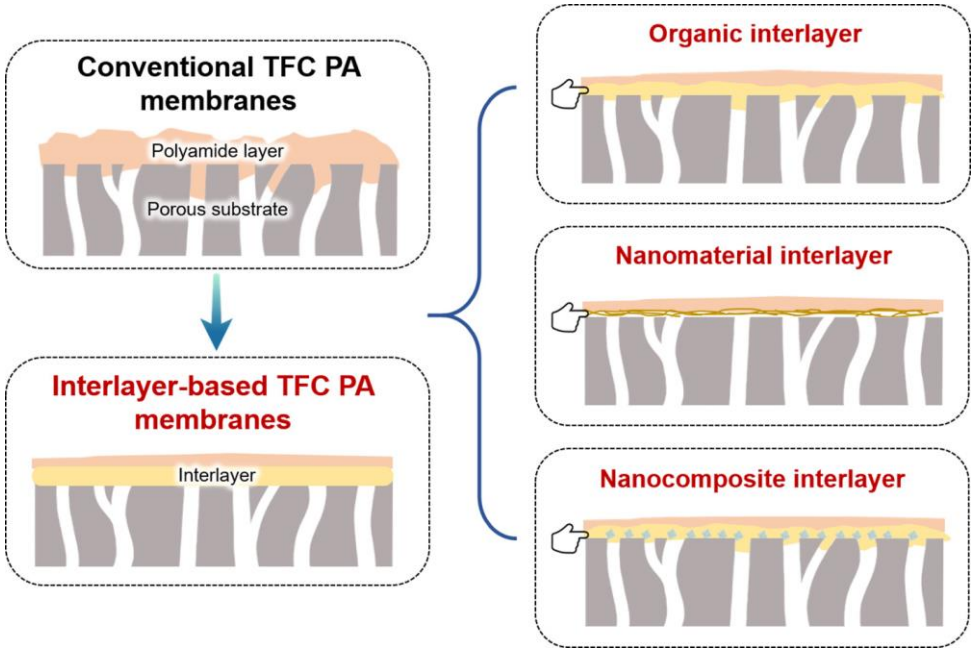

Figure 10 Types of interlayers [45]

Various studies have incorporated the use of interlayers to enhance membrane performance. Tannic acid (TA) has been studied as an organic interlayer, as it forms a stable, non-toxic complex with Fe^{3+}, that is easy to synthesize. This TA-Fe interlayer has been used on challenging PTFE substrates, creating an even PA layer with minimal defects, while overcoming the seemingly inevitable permeability-selectivity trade-off [11]. Single wall carbon nanotubes (SWCNTs) have also been studied to provide uniform nanoscale pores with high porosity and a smooth surface morphology [46]. They had also shown good stability in harsh aprotic solvents such as DMF [8]. Other interlayers such as $Cd(OH)_2$ nanowires [47] and metal organic frameworks (MOFs) [48] have also been studied. The downside of such having such interlayers is that although some might be easy to synthesize, it is still an addition step in the membrane fabrication process. The number of steps for the fabrication should be as few as possible to make the process desirable for future scale up and commercialization.

2.7 Research gap

As discussed, there is a lack of solvent resistant polymeric membranes for the OSN of harsh aprotic solvents. Previously synthesized polymeric membranes for these purposes require addition steps such as crosslinking or interlayer formation, making them unfavorable for commercialization. As such, the author focused their research on developing chemically resistant membranes for the OSN of strong solvents such as DMF and DMSO as these are commonly used solvents in the industry [49].

PTFE, commonly known as Teflon, is a promising material for this purpose as its C-F bonds are one of the strongest known single bonds. This not only provides for its excellent chemical resistance, but also for its high mechanical strength [50]. The author intends to harness the chemical stability and mechanical strength of PTFE to synthesize a robust membrane for the OSN of aprotic solvents. By doing so, the extra crosslinking step necessary for most other polymeric OSN membranes can be voided. However, due to its inert nature, PTFE membrane fabrication is limited to sintering, spinning and extrusion methods, which result in a porous membrane structure, with pores in the microfiltration range [15, 51]. Controlling the pore size during this process is difficult. As such, the resulting PTFE membrane would have pores in the microfiltration range. To make these substrates fit for OSN, a thin polyamide film can be synthesized on top of the PTFE support, forming a polyamide-PTFE TFC where the polyamide layer provides for the membrane selectivity and the desired properties of PTFE are retained.

Prior to synthesizing the polyamide layer, the PTFE substrate would have to undergo surface modification. PDA coating was determined as the most appropriate as it is simple and easier to carry out as compared to other surface modification procedures. This polyamide layer can be synthesized via interfacial polymerization. However, the uneven pores on PTFE make it challenging. As shown, previous studies have employed the additional step of using interlayers to overcome this issue. However, in a recent study, Y. Zhong. et al. synthesized a defect free polyamide layer on a flat sheet PTFE substrate using a novel two-time IP technique, without the use of interlayers [52]. In this technique, after introducing the aqueous phase to the substrate, the organic phase was poured onto the flat sheet twice, with heat treatment between

each pour. Upon the first TMC and heat treatment, Zhong observed that there were droplets of the aqueous layer remaining on the substrate, indicating that a second round of IP is possible with exposure to just the organic phase alone. It was hypothesized that upon heat treatment, the aqueous phase in the substrate pores gets pulled up by interfacial tension, explaining the observed droplets. Hence, instead of the additional step of synthesizing an interlayer, the author adopted this IP method for the synthesis of PTFE-PA hollow fibre membranes. Details of this synthesis can be found in section 3.2. This is also the first study that uses PTFE hollow fibre membranes for the purification of harsh aprotic solvents.

3 Experimental

3.1 Materials

PTFE hollow fibers were supplied by Zhejiang ECO Environmental Technology Co. Ltd and the inside out configuration was used. The PTFE substrates had an inner diameter of 470 μm and were cut into 12 cm long fibers for polyamide thin film synthesis. Four of such fibers were used in each membrane module. Dopamine hydrochloride (Sigma Adrich) and tris(hydroxymethyl)aminomethane (Tris, >99.8%, Sigma Aldrich) were used for surface modification of the PTFE membranes. Branched polyethyleneimine (PEI) with molecular weights 800 Da (Polyscience), 75,000 Da (30 wt% in aqueous solution, Polyscience) and 750,000 Da (50 wt% in aqueous solution, Sigma Aldrich), piperazine (PIP, 99%, Merck), sodiumdodecylsulfate (SDS, 99%, Sigma-Aldrich), trimesoyl chloride (TMC, 98%, Sigma-Aldrich), and cyclohexane (99.5%, Merck) were used in the polyamide layer synthesis. N,N-dimethylformamide (DMF), dimethyl sulfoxide (DMSO) and acetonitrile (ACN) solvents as well as sudan orange (SO, 85%), methyl orange (MO, > 85%), acid fuchsin (AF, 70%) and rose bengal (RB, >95%) dyes used in the solute-solvent system were purchased from Sigma Aldrich. Deionized water (Milli-Q, 18 MΩ cm) was used for the aqueous solution preparation. Figure 11 shows the structure of the aqueous and organic monomers used in IP.

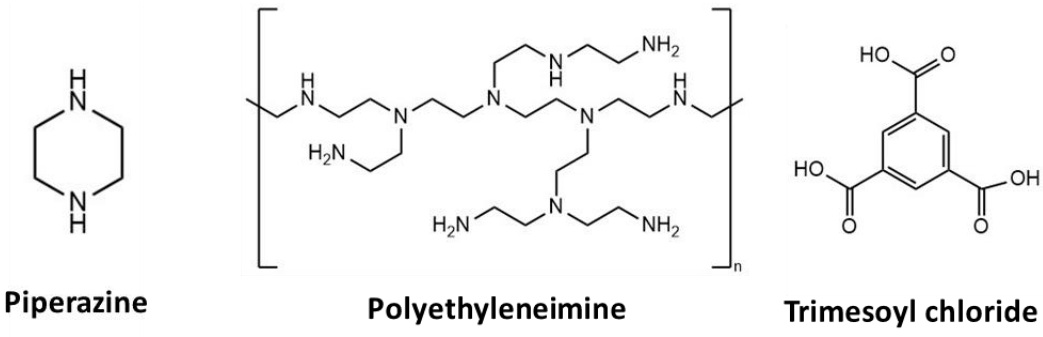

Figure 11 Structure of monomers used

3.2 Membrane synthesis

3.2.1 PDA functionalization

Prior to polyamide synthesis, the inner surface of the substrate was modified with PDA to improve its hydrophilicity. A polydopamine (PDA) solution containing 1g/l polydopamine and 50mM of tris(hydroxymethyl)aminomethane was circulated through the lumen of the hollow fibres at 80 ml/min for 30 min. There were two methods employed for the PDA coating: with and without catalyst. The above describes the scenario without catalyst use. If catalysts were used, $CuSO_4$ and H_2O_2 would be added into the PDA solution above. The modified substrates were then rinsed with DI water. A polyamide thin film layer was then synthesized on the inner surface of the modified hollow fibres via interfacial polymerization as described in section 3.2.2.

3.2.2 Polyamide synthesis

There were three methods employed to synthesize the polyamide layer before the best method could be chosen. They are the single layer, double layer, and two-time IP methods.

For the single layer method, an aqueous solution containing PEI (0.8, 75 or 750k Da) and/or PIP with a small amount of SDS was first prepared and stirred for 2 hours. The aqueous solution was introduced into the lumen of the PDA coated substrates using a syringe and was left to soak for 20-30 min. Excess aqueous solution was then washed off by purging the lumen with cyclohexane at 60 ml/min using a peristaltic pump for 2 min. Then, the organic phase reactant containing TMC (0.10 or 0.15 wt%) in cyclohexane was pumped through the lumen of the substrates at 20 ml/min for 2 min for the interfacial polymerization reaction to take place.

For the double layer IP method, after TMC was introduced, the aqueous phase was introduced into the lumen again and subsequently flushed with cyclohexane and TMC once more for the same duration and flow rate.

The two-time IP process differs from this, and the process is as follows. After soaking the PDA coated substrate in the aqueous phase and purging with cyclohexane, TMC is circulated through the fibre lumen for just 1 min, then heat treated in a 60 ºC oven for 5 min. After which, TMC is circulated through the fibre for 1 min again and heat

treated a second time. This two-time IP method was deemed as most ideal and will be further discussed in section 4.4. After the IP process, the membrane was left to stand for 10-20 min, rinsed and stored in DI water. Table 2 below shows the summary of the conditions used for the three methods.

Table 2 Method conditions for polyamide synthesis

Method	**Aqueous phase soak time (min)**	**1st cyclohexane flush time (min)/ rate (ml/min)**	**1st TMC flush time (min)/ rate (ml/min)**	**Heat at 60°C for 5 min**	**2nd cyclohexane flush time (min)/ rate (ml/min)**	**2nd TMC flush time (min)/ rate (ml/min)**	**Heat at 60°C for 5 min**
Single layer	20-30	2/ 60	2/ 20	No	-	-	No
Double layer	20-30	2/ 60	2/ 20	No	2/ 60	2/ 20	No
Two-time IP	20-30	2/ 60	1/ 20	Yes	-	1/ 20	Yes

3.3 Characterization

3.3.1 Scanning Electron Microscope (SEM)

SEM is a technique that uses electron beams to image small samples, allowing for a high image resolution and a magnification of up to 500,000 times [53]. These images can go down to the micron level, allowing us to view the roughness, thickness, and uniformity of the polyamide layer. The samples need to be conductive and free of moisture as the SEM operates in vacuum. As the membrane used in this study was not conductive, it was first coated with platinum prior to analysis. This allowed for the surface topography, as well as the cross-section morphology to be analyzed. XPS was also used to visually confirm that the thin polyamide layer had been formed and deduce its estimated thickness. One downside to this technique is that it may not be representative of the whole sample as only a small area can be analyzed.

3.3.2 Porometer

There are many ways to measure membrane pore size, including techniques such as thermoporometry and permporometry, each with their own pros and cons. For this study, capillary flow porometry was used to evaluate the pore size distribution and permeability characteristics of the material. The sample pores are first filled with a wetting liquid and gas is blown to slowly empty the pores, starting from the largest. The flow of the gas is then measured, and pore size can then be calculated according to the Washburn equation. A schematic of a capillary flow porometer is shown in Figure 12 below.

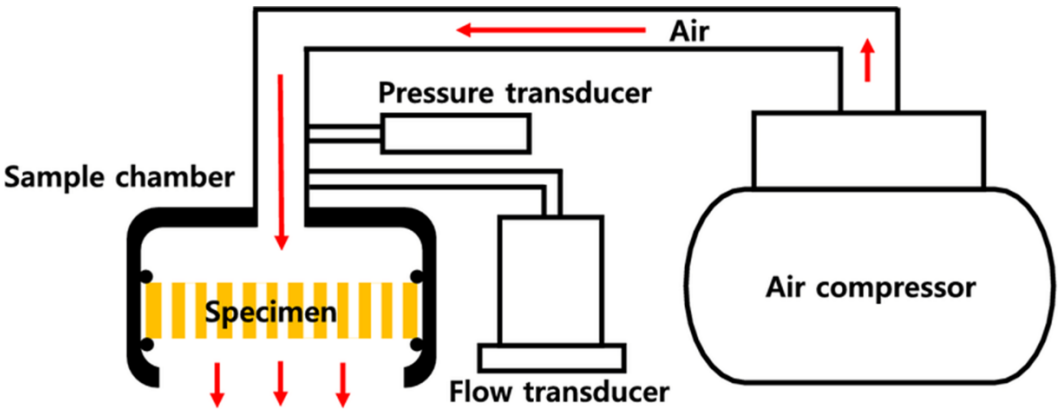

Figure 12 Schematic diagram of a capillary flow porometer [54]

It is to be noted that this technique was used to determine the pore size distribution of the PTFE substrate. To obtain pore size of the synthesized polyamide-PTFE nanofiltration membrane the absolute filtration method was used, whereby solutes of different sizes were filtered to obtain the MWCO. The above-mentioned techniques cannot be used due to the absence of physical pores within the polyamide matrix.

3.3.3 Tensile testing

Tensile testing is done to determine the strength of a sample by subjecting it to a stress until the material fails/ breaks. The stress over strain curve can be plotted and the behavior (elastic/ plastic) can also be visualized. The tensile strength of the membranes was measured by clamping the ends of the substrate and elongating it along its length. The stress over strain graph was plotted and tensile strength and yield strength values were obtained from the measurements.

3.3.4 Contact Angle

The contact angle given information on how hydrophobic or hydrophilic a surface is. It is the angle between the solid-liquid and liquid-gas interface, where surfaces with a contact angle of more than 90 are considered hydrophobic, and those less than 90 are considered hydrophilic. There are two ways contact angles can be measured. The first way is by placing a small drop on the surface and measuring the angle. This is known as the static contact angle. Another way is to measure the contact angle during movement [55]. This angle is known as the dynamic contact angle. In this study, the dynamic contact angle was studied, where the fibre was immersed and emerged from a water bath and the advancing and receding contact angles can be recorded. Other than the nature of the material, the contact angle is also affected by other factors, such as surface roughness, chemical inhomogeneity of the surface and/or wetting liquid and temperature [56].

3.3.5 Fourier-Transformed Infrared Spectrometer

In FTIR, the sample is subjected to infrared radiation at various frequencies which cause specific bonds to vibrate. These are then recorded as wavelength against transmittance to identify the functional groups present in the sample. FTIR was used to chemically confirm the formation of the polyamide selective layer with the presence of the amide functional group. Prior to measurement, the sample must be dried to

prevent loss of data with peaks buried under the water peak. One downside to this technique is that it is unable to detect trace elements.

3.3.6 X-ray Photoelectron Spectrometer (XPS)

XPS is a quantitative technique that can tell the elemental composition of a sample. It is a surface analysis technique that can analyze up to 10nm in depth [57]. It uses an x-ray beam to excite the molecules on the sample surface, causing a photoelectron emission. These photoelectrons are analyzed and gives information on the binding energy, which is element specific. The upside to using XPS over FTIR is in its ability to detect elements at lower concentrations. The XPS was used to confirm the presence of PDA, polyamide, and the adsorption of the aqueous phase onto the substrate. Figure 13 below shows the schematic diagram of an XPS set up.

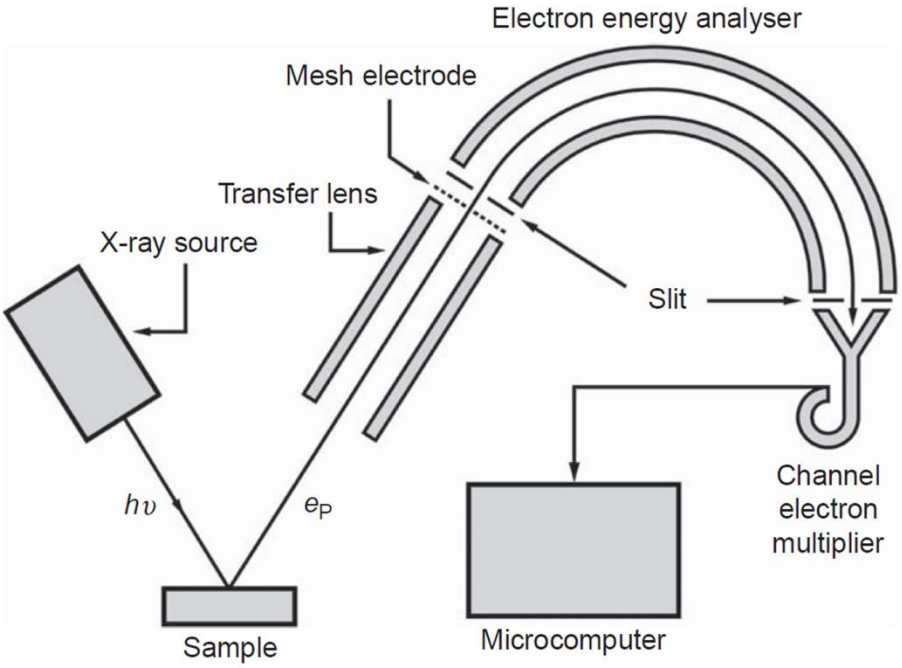

Figure 13 Schematic diagram of an XPS measurement system [58]

3.3.7 Surface charge

When a charged object is exposed to an electrolyte, the ions in the electrolyte interact with the charged surface and form an electric double layer. The first layer, known as the stern layer, consists of an immobile layer of ions that are of the opposite charge to that of the object. The second layer, known as the diffuse layer, comprise of loosely

held ions attracted to the charged surface via electrostatic charges. Figure 14 shows an illustration of the electric double layer formed around a negatively charged particle.

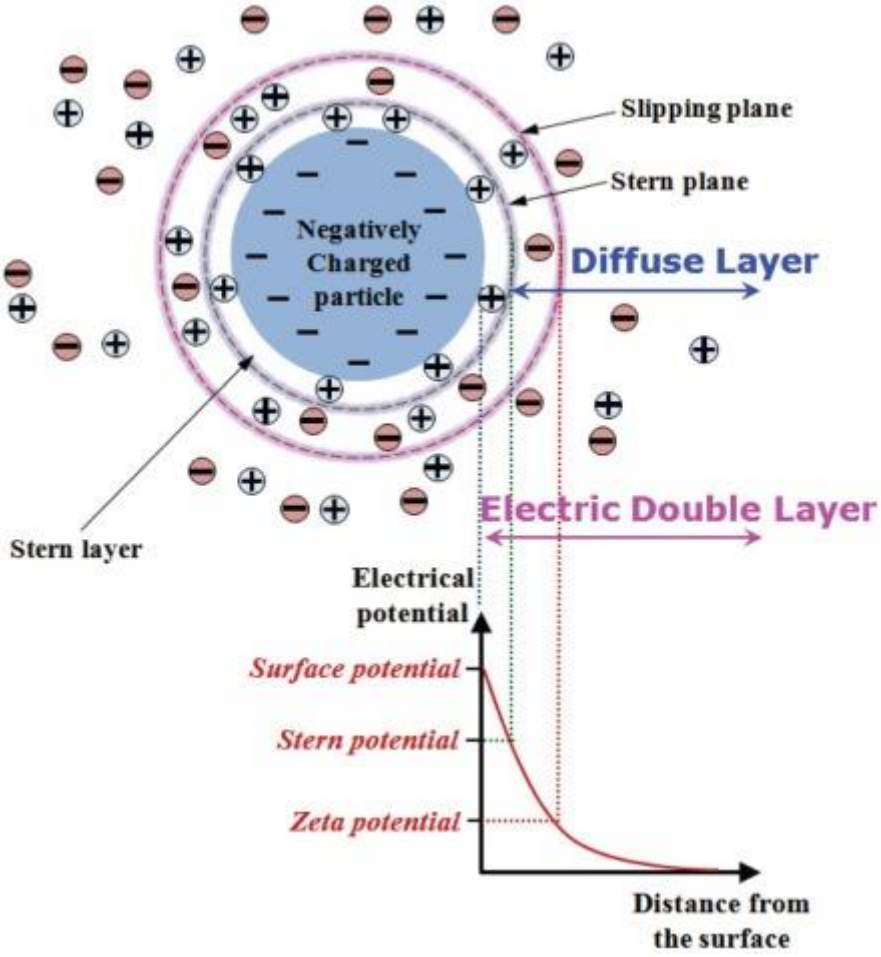

Figure 14 Illustration of electric double layer [59]

The surface charge can be characterized trough zeta potential measurements. Though the zeta potential cannot be measured directly, it can be deduced through experiments by means of a model [60]. Knowledge of the membranes charge would help in explaining certain membrane behavior and in determining the membrane's applications. Streaming potential is one way to measure zeta potential, and it is the potential difference at the point where no current is produced by the flow of charge due to a pressure gradient through the membrane [61]. The zeta potential is often plotted against pH and pH at which the zeta potential is zero is known as the isoelectric point.

3.4 Performance tests

Pure water was circulated through the lumen of the membranes and permeation was measured in a crossflow mode. The membrane was allowed to undergo compaction for at least 1 hour, at an effective transmembrane pressure of 2 bar, before the steady state permeation flux was measured. Two membrane samples per formulation condition was tested to obtain an average water permeation flux. The pure water permeability, PWP ($Lm^{-2}h^{-1}bar^{-1}$) was calculated using the equation:

$$PWP=F\Delta P=QA\Delta P \qquad \text{-(1)}$$

where F is the permeation flux (L m^{-2} h^{-1}), ΔP is the transmembrane pressure (bar), Q is the volumetric permeation flow rate (L h^{-1}) and A is the effective membrane area (m^2).

The membranes were also tested for dye rejections using various dyes such as sudan orange, methyl orange, acid fuchsin and rose bengal, in DMF solvent. The membranes were tested at 2-3 bar. The solute rejection, *R* (%) was calculated using the equation:

$$R = \left(1 - \frac{c_p}{c_f}\right) \times 100\% \qquad \text{-(2)}$$

where, C_p and C_f are the concentrations of the permeate and feed solutions, respectively. According to the Beer-Lambert law [62], the permeate and feed concentrations can be determined by UV-Vis Spectroscopy since solution concentration is proportional to light absorbance. It is important to note that the dyes could also be charged, affecting the apparent rejection depending on the membrane surface charge. In this case, the four mentioned dyes used are negatively charged [63]. Figure 15 shows the chemical structures of the dyes used.

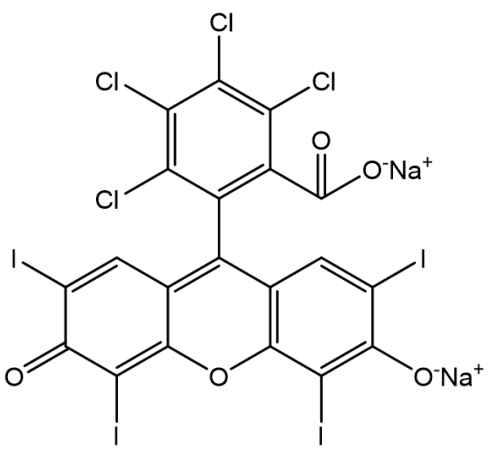

Rose Bengal

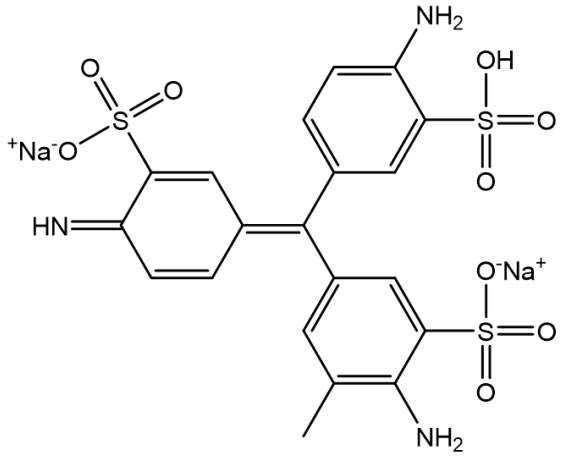

Acid Fuchsin

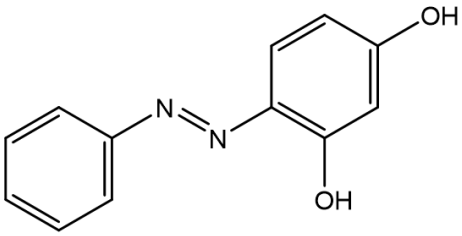

Sudan orange

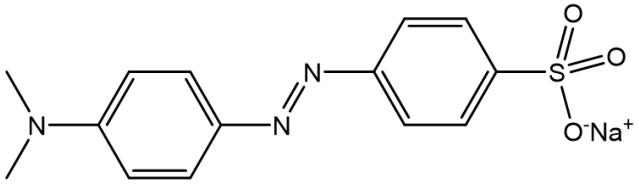

Methyl orange

Figure 15 Chemical structure of dyes used

4. Results and discussion

4.1 Substrate Characterization

Zhejiang ECO Environmental Technology Co., Ltd provided two sets of PTFE hollow fibre substrates and their cross sections and inner surface morphology was imaged using SEM as seen in Figure 16. From the surface morphology of the pores, it can be deduced that the fibres were formed through the hot-melting and stretching fabrication methods.

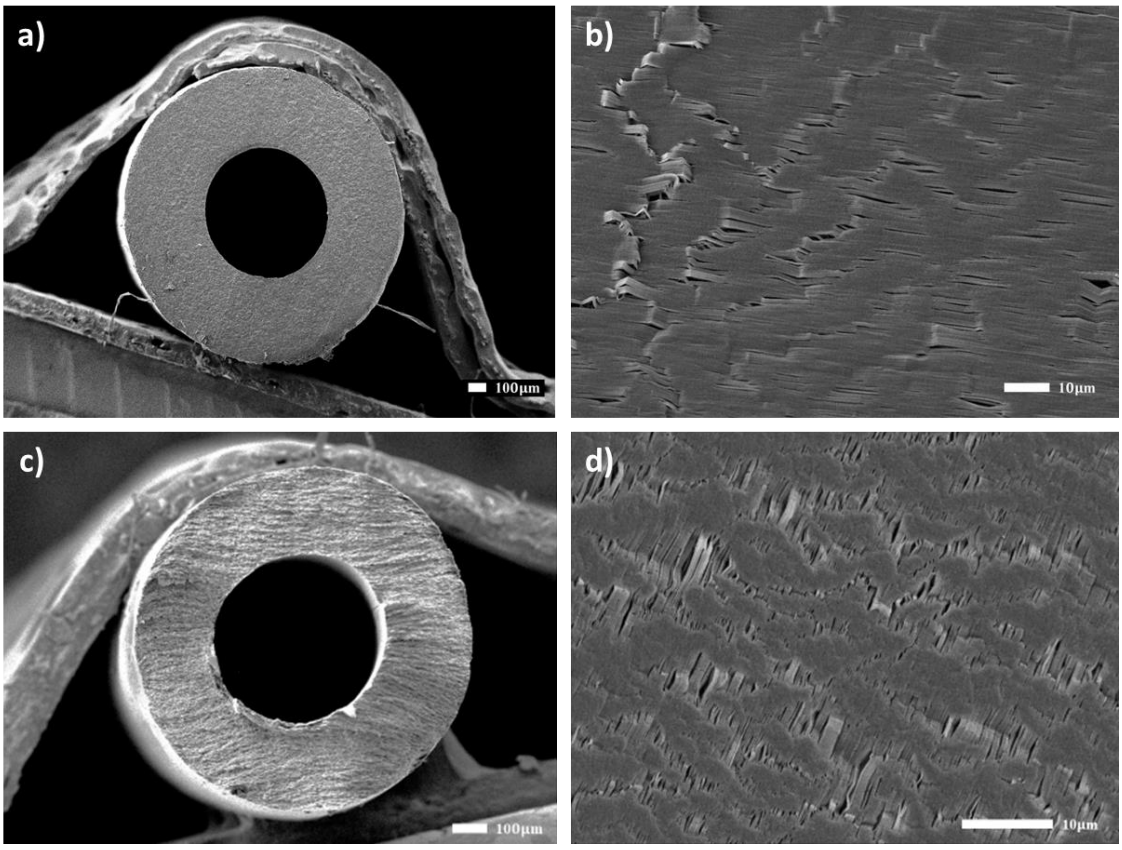

Figure 16 SEM images of PTFE substrate surface

Figure 16a-b show the first batch of hollow fibres (B1) that had an inner diameter of 715 μm, and pores ranging from 0.1μm to more than 10μm in length. Figures 16c-d show the second batch of hollow fibres (B2) that had in inner diameter of 470 μm, and pores ranging from less than 1 μm to 5 μm in length. B1 had a more irregular surface morphology with smooth and rough areas, while B2 had a more uniform morphology. As such PTFE hollow fibre substrates from B2 were used in this study as it would be easier to form the polyamide layer on top of a more uniform substrate. The water and DMF permeations of the pristine substrates were also tested and were found to be 360 and 306 $lm^{-2}h^{-1}bar^{-1}$ respectively.

The fibre's tensile strength was measured and the graph of tensile stress over strain was plotted as shown in Figure 17. The tensile strength (the maximum stress a material can withstand) of the PTFE fibre was around 34.1 MPa and its yield strength (the point where the curve deviates from proportionality) was approximately 17.1 MPa. These values are higher than hollow fibres of other materials such as PES [23] PI [22] and even PVDF [64]. It should be noted that several samples were tested, and the reported values are the average of those measurements.

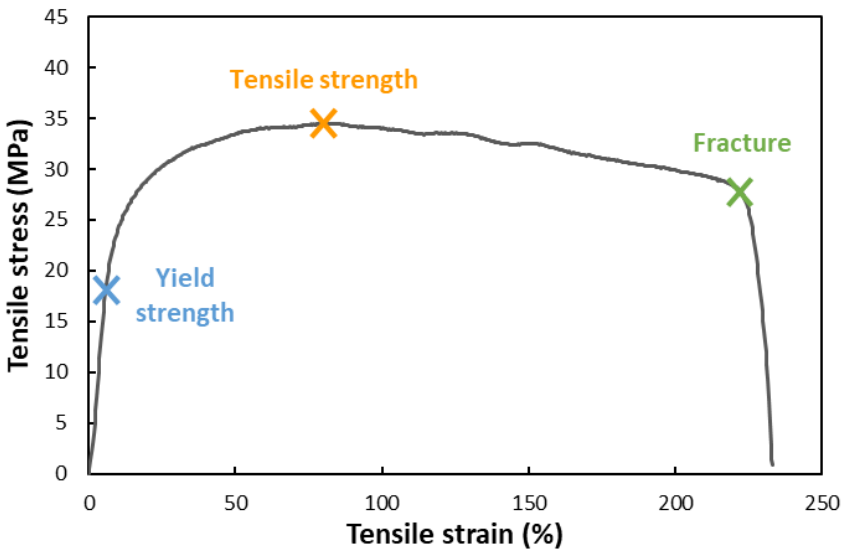

Figure 17 Tensie test curve of PTFE hollow fibre

The pore size distribution of the substrates was measured, and the pore size distribution graph was plotted as seen in Figure 18. The substrate had a mean pore size of around 133 nm. Although the graph does show a sharp peak at 133 nm, only 24.4% of pores were this size. This shows that the substrate's pore size distribution is still relatively large, having pores up to 320 nm in size.

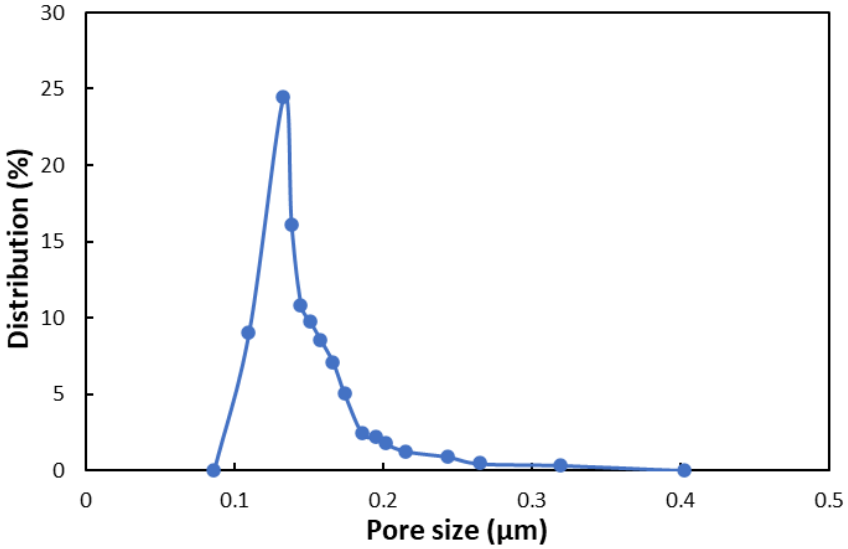

Figure 18 Pore size distribution of PTFE hollow fibre

4.2 Substrate Modification

As mentioned, PDA functionalization of the PTFE substrate is necessary to increase its hydrophilicity prior to interfacial polymerization. Several attempts were made to coat the substrate surface in attempts to find the optimal PDA condition, and these conditions are summarized in Table 3.

Table 3 PDA coating conditions used

Coating no.	Dopamine	$CuSO_4$	H2O2	Time	Solvent
C0	2 g/L	5 mM	19.6 mM	15 mins	Water
C1	2 g/L	2.5 mM	9.8 mM	15 mins	Water
C2	2 g/L	-	-	20 mins	Water
C3	1 g/L	-	-	20 mins	Water
C4	2 g/L	5 mM	19.6 mM	15 mins	20wt% IPA
C5	2 g/L	-	-	20 mins	20wt% IPA
C6	1 g/L	-	-	20 mins	20wt% IPA

The first coating attempt was made using the initial conditions (C0). The procedure as mentioned in section 3.2.1 was followed, and the SEM images of the initial coated membrane surface can be seen in Figure 19.

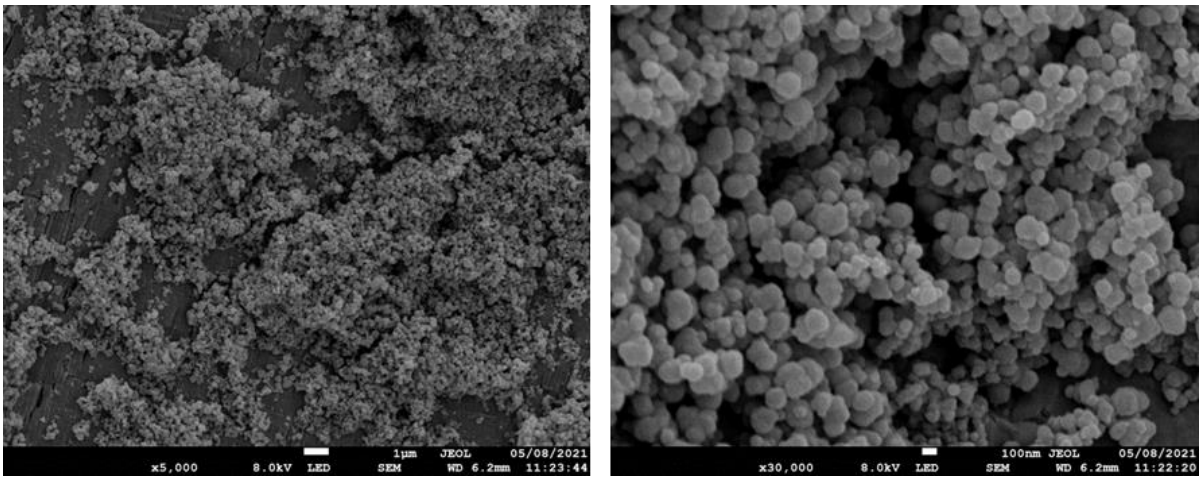

Figure 19 Overall and close view of initial PDA deposition (C0)

From the images, the PDA agglomerations are more than 100nm in size and form a thick, uneven ‘cakey’ layer on top of the PTFE substrate. This rough surface would affect the interface for IP and make it difficult for the synthesized polyamide layer to adhere well onto the substrate. Subsequent attempts to optimize PDA deposition included the use of IPA in the solution and carrying out the polymerization in the absence of catalysts. These changes are further discussed in sections 4.2.1 and 4.2.2.

4.2.1 With pure water as solvent

For these set of membranes, 100% MilliQ water was used as the solvent. Figure 20 shows the SEM images of the PDA coated membrane surfaces of the corresponding formulations. Parameters such as the dopamine concentration, amount of catalyst used, and reaction time were studied. All three substrates (C1, C2, C3) appeared to have fewer PDA deposits than C0. The PDA deposits when comparing images C1b and C2b are similar, suggesting that an increase in time compensates for the absence of catalyst. When preparing the dopamine solution using the initial conditions as stated in C0, the dopamine solution turned from colorless to dark brown within a few seconds upon the addition of dopamine. However, when no catalyst was used it took approximately 10 mins for the same color change. This is a shorter time as compared to that stated in literature, where the color change was observed only after several hours [44].

Although it was hard to view from the SEM, there were small PDA agglomerations on the substrate of C3. This is close to the ideal deposition amount where there is just enough to prevent delamination of the polyamide layer and not too much to hinder the polyamide layer formation. The substrate lumen also changed color from white to light brown indicating that PDA had been deposited on the hollow fibre. Out of the three, C3 had the most ideal PDA deposition. Overall, the trends for PDA deposition in water were predictable and controllable making it easy to repeat.

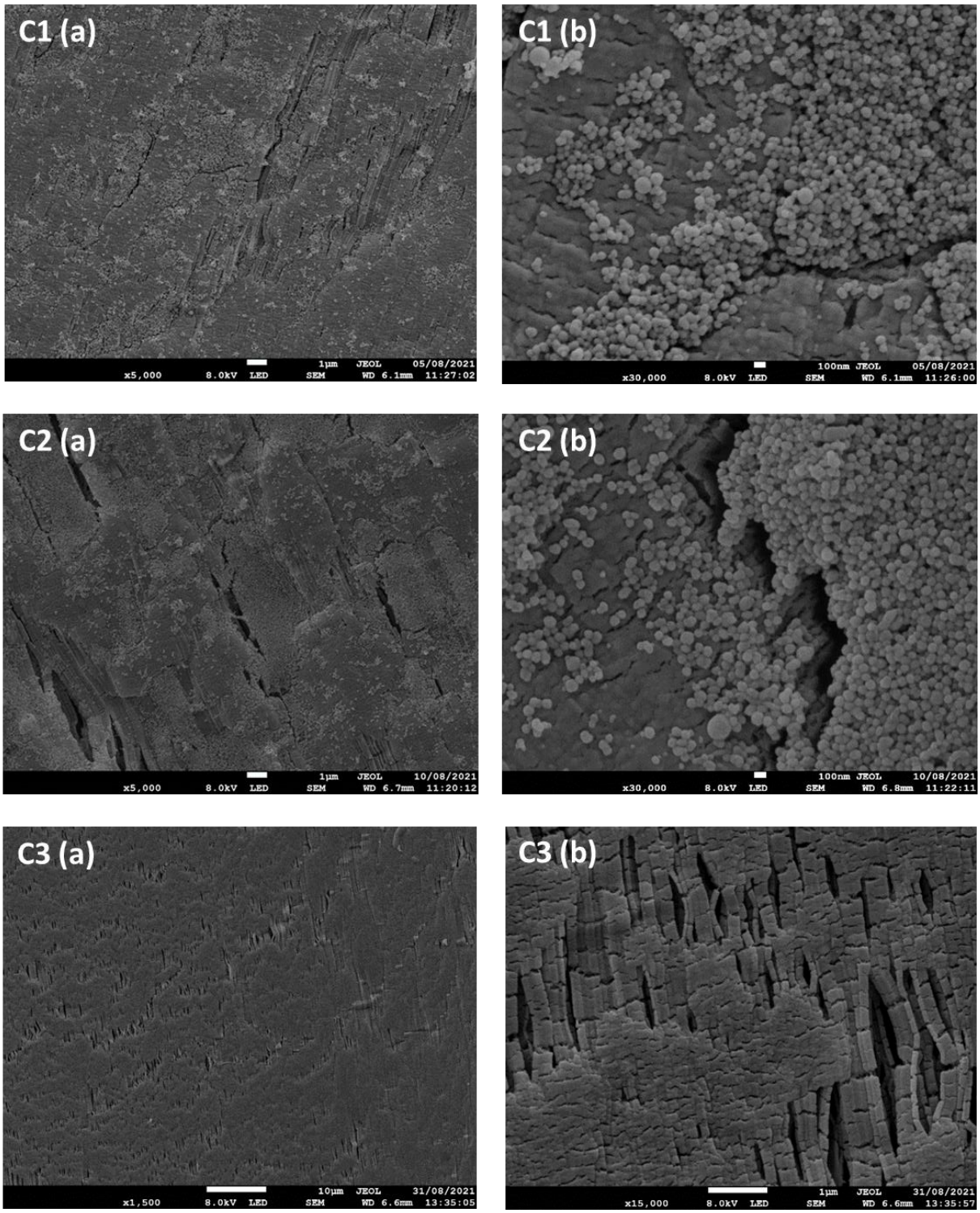

Figure 20 (a) Overall and (b) close view of PDA coating with water as solvent

4.2.2 With 20 wt% IPA as solvent

It was hypothesized that IPA could reduce the interfacial surface tension between PTFE and water, allowing for the PDA solution penetrate the pores better so that the substrate's hydrophilicity can be improved throughout its depth and not solely at the surface. It was noted that at 20 wt% IPA there was a drastic drop in surface tension while further increments of IPA did not result in much significant change [65]. As such, for the following membranes, 20 wt% IPA in water was used as the solvent.

As seen from the SEM images in Figure 21, all three substrates (C4, C5, C6) had fewer PDA deposits than C0. By comparing C4 to C0, the PDA deposition has been reduced greatly just by introducing IPA into the solution. According to Jiang et. al., the reactants (dopamine) are more soluble than the product (PDA) in water, shifting the equilibrium to generate more PDA [66]. When 20 wt% alcohol is added as part of the solvent, the PDA spheres increased in size. However, this was not observed in this experiment, where the size of the PDA spheres remained relatively unchanged, with and without the use of IPA. In C5b, the spherical PDA spheres are joined together and not well defined. From literature, this was only observed at higher concentrations of alcohol of around 50% and above Generally, the PDA spheres are more defined when IPA was not incorporated into the solvent. This is because PDA is more soluble in the 20 wt% IPA solution than in pure water [66].

Half the amount of dopamine was used in C6 as that in C5. Although difficult to see, there are some PDA deposits on the substrate in M89, making it ideal. It was interesting to note that the best coating in water and in 20 wt% IPA had the same conditions. Between the two types, generally, PDA deposition in water was easier to control and the results were more predictable and repeatable. Some observations of dopamine in 20wt% IPA in this experiment also did not corelate with that in literature, making the conditions in C3 more ideal due to its repeatability. As such the conditions in C3 were deemed as the most ideal for the PDA coating step.

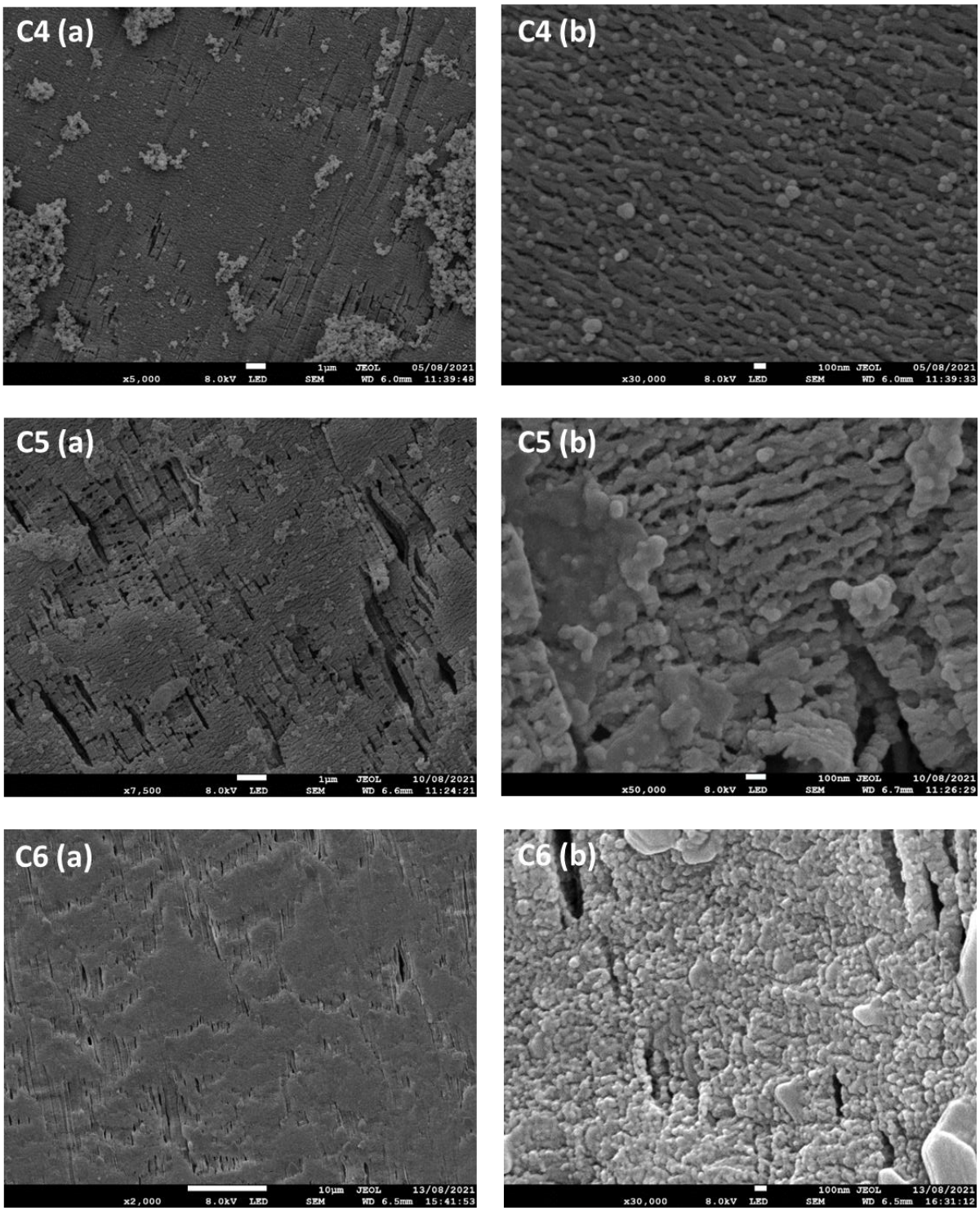

Figure 21 (a) Overall and (b) close view of PDA coating with 20 wt% IPA as solvent

4.2.3 Contact angle measurements

The dynamic water contact angle of the modified and unmodified substrates was measured. Upon modification, the average contact angle dropped from 105.4° ± 2.3° to 85.8° ± 2.8°. A contact angle above 90° is considered hydrophobic and less than 90°, hydrophilic. Although the change in contact angle is minimal, it is known that improvements in hydrophilicity is often limited due to the low surface energy of PTFE [42]. The roughness of the substrate could also play a part in the high contact angle. Nevertheless, a drop of about 20° is common for PTFE modification [10, 42].

In this study, the inner surface (lumen) of the hollow fibre was functionalized. For the static contact angle to be taken, the fibre would have to be cut open longitudinally and flattened, potentially changing the surface structure and 'cracking' the surface PDA coating. To prevent this, the outer surface of the hollow fibre was coated for the dynamic contact angle to be measured. The inner and outer surfaces of the substrate may differ in pore structure, size, and roughness. As such, the contact angles recorded would likely represent the qualitative improvement in hydrophilicity rather than a quantitative one.

4.2.4 Chemical analysis of PDA coating

XPS analysis was carried out to study the PDA coating and the subsequent adsorption of the aqueous monomers onto the substrate surface and the results can be seen in Figure 22. There are three spectra shown: the pristine PTFE substrate, PDA coated substrate and the PDA coated substrate after immersing in the PEI aqueous phase. After soaking the substrate in PEI, the hollow fibre was purged with cyclohexane and dried prior to analysis. The increase in the O1s (531.1 eV) and N1s (398.1 eV) peaks upon PDA coating suggests that PDA has been successfully deposited onto the PTFE substrate surface. By comparing the PDA coated spectrum to the PEI adsorption spectrum, the N/O ratio increased from 0.16 to 0.62. PEI monomers only contain C and N elements, so the increase in N/O ratio indicates that the PEI monomers adhered onto the PDA coated substrate.

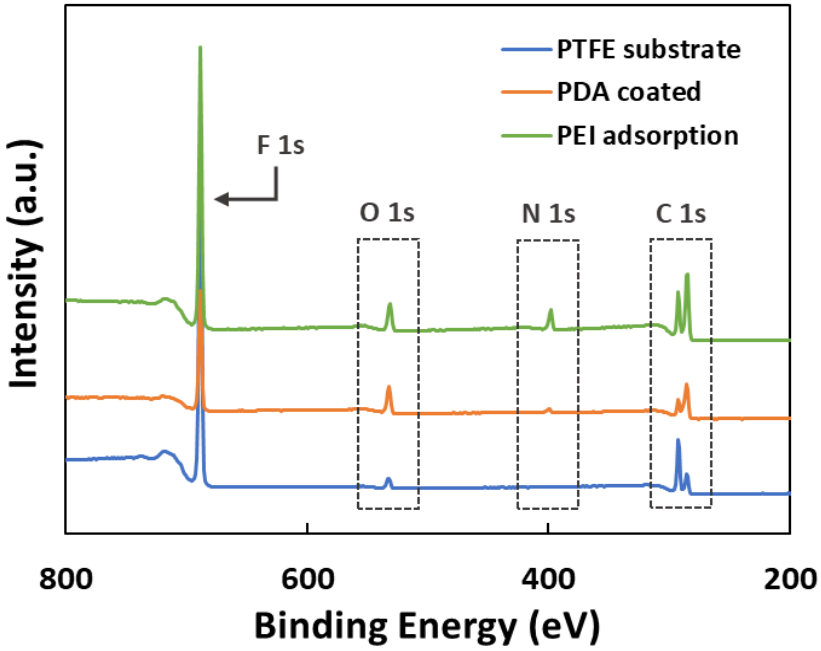

Figure 22 XPS wide scan of PTFE fibre, PDA coated substrate and PEI immersed substrate

4.3 Aqueous monomer types

As mentioned in section 2.4, there are several possible monomers one can use to make the polyamide layer. Three of such monomers were explored: PEI, PIP and MPD. This section focuses on the type of polyamide selective layer formed with these monomers and identifying the best monomers to be used for this study.

4.3.1 PEI type polyamide

PEI is a positively charged monomer commonly used in polyamide thin film synthesis. These monomers come in various molecular weights and are usually branched. They also form a looser network as compared to that of the MPD type polyamide. Usually, the PEI type monomers form a polyamide layer with either a smooth surface or one with large rings. Figure 23 shows the smooth surface morphology of the PEI type polyamide.

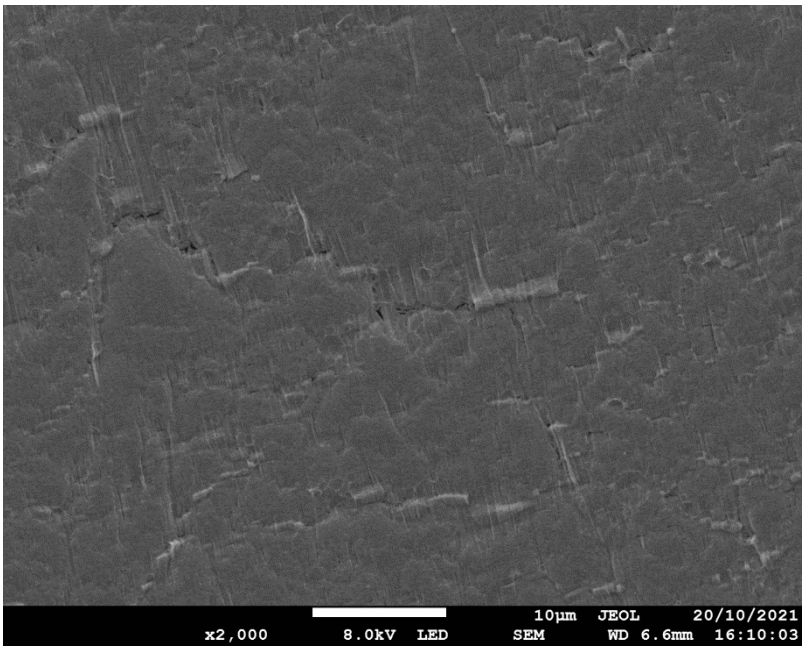

Figure 23 SEM image of PEI type polyamide

4.3.2 PEI-PIP type polyamide

Typically, such polyamide layers are composed mainly of PEI with only small amounts of PIP used in comparison. PIP is added into the system to increase crosslinking and in turn reduce the MWCO of the membrane. Figure 24 shows the SEM image of two PEI-PIP type membranes, one with a higher PIP concentration of 0.04 wt% and the other with a lower concentration of 0.02 wt%.

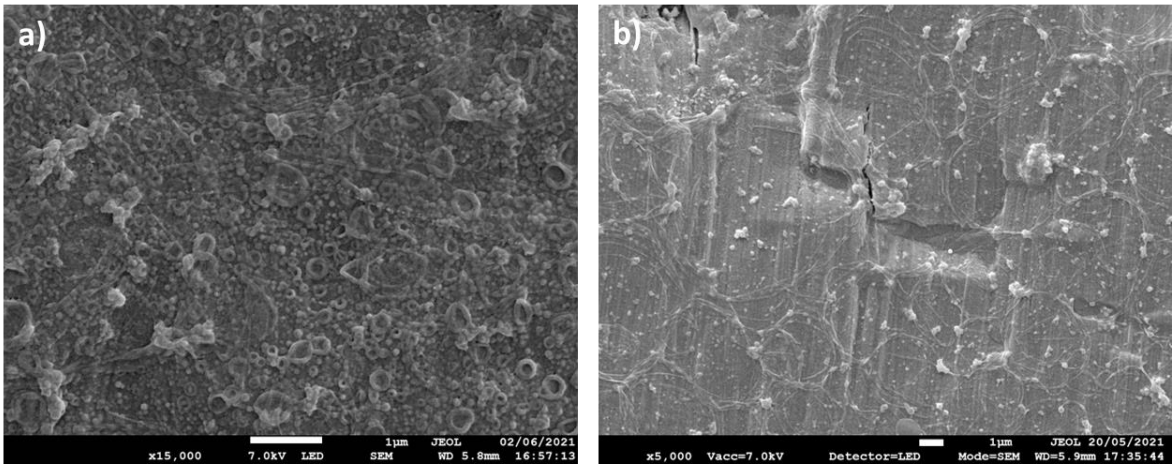

Figure 24 SEM images of PEI-PIP type polyamide layer with a) 0.04 and b) 0.02 wt% PIP

PIP and PEI based polyamide have distinct morphologies, with PEI having a smoother ring like structure and PIP having a rougher morphology. In Figure 24a, the PIP structure is more visible, with a rough surface with small donut like structures, round with an indentation in the center. In Figure 24b, when less PIP was used, the PEI structure becomes more visible with ring like folds along the surface. The PIP morphology is more obvious up close while PEI is better seen when observing the overall surface. During IP, the larger PEI macromolecular monomers diffuses from the pores to the interface at a slower rate due to its larger size and slower reactivity with TMC as compared to PIP [67, 68]. Hence, PIP reacts first, while PEI reacts later, creating a layer on top of the initially formed PIP-polyamide layer [35, 67]. The PIP-PEI ratio also plays a part in the morphology of the resultant polyamide layer. It was shown in a previous study that for the same aqueous monomer concentration, higher amounts of PEI resulted in a thicker polyamide layer [69]. Not only does the PIP-PEI ratio affect morphology, but it also affects the charge and overall polyamide performance.

4.3.3 MPD type polyamide

MPD is a common monomer used in reverse osmosis membranes due to its low MWCO. These membranes tend to have large, rough, ‘leaf-like’ structures that increase the filtration surface area and in turn, increase permeability [70]. Figure 25 shows the SEM image of the synthesized MPD type membrane. The downside noticed for this type of membrane was the overall lower permeability due to the lower MWCO and the need for larger concentrations of MPD (up to 6 wt%) to achieve complete coverage of the substrate surface.

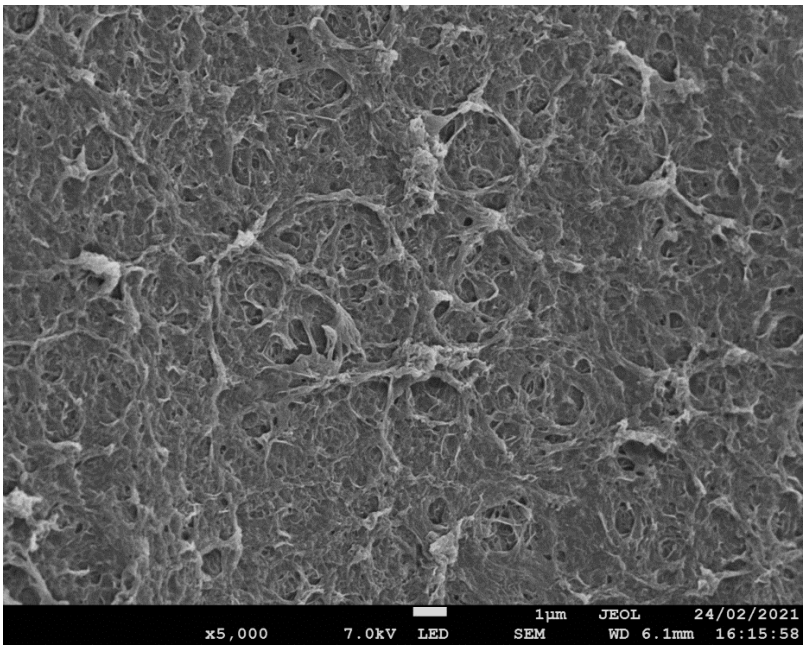

Figure 25 SEM image of an MPD-type polyamide surface

4.3.4 PEI-MPD type polyamide

Although these MPD and PEI are not commonly used together, it was hypothesized that the PEI could help in the formation of a defect free polyamide layer without the use of high concentrations of MPD. Figure 26 shows the image of a PEI-MPD type membrane, where better coverage was achieved when just 1 wt% of MPD was used.

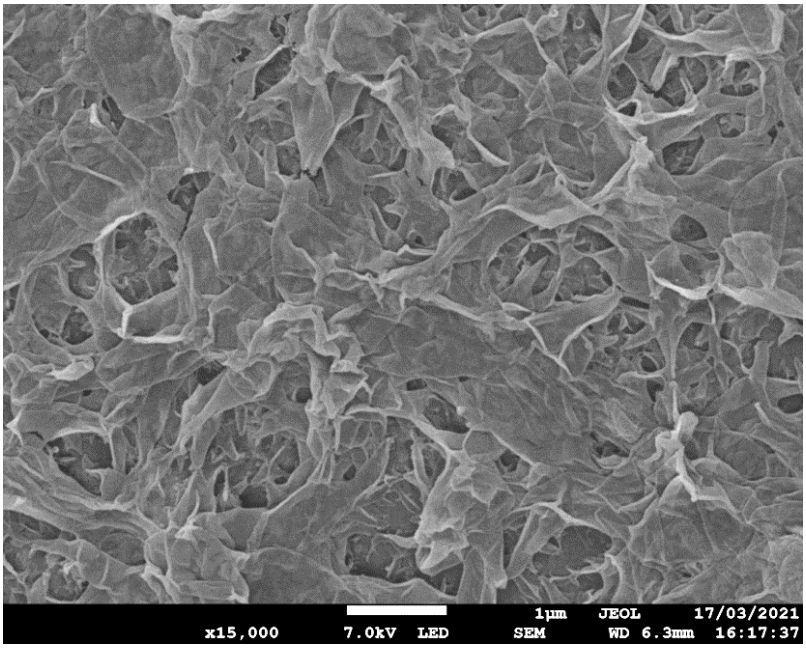

Figure 26 SEM image of a PEI-MPD type polyamide surface

Upon closer inspection it was observed that the polyamide film had several layers to it, which could be due to one of the monomers taking a longer time to diffuse than the other. The morphology of the mixed monomer polyamide layer seems to have a combination of both the PEI and MPD type polyamide.

Eventually the PEI type and the PEI-PIP type polyamide was chosen due to the lower concentration of starting reagents and better reproducibility. One other benefit was the ability to control the MWCO of the polyamide by varying the PIP concentration, allowing the membrane to be tailored to its desired use.

4.4 Polyamide coating optimization

As mentioned in section 3.2.2, the author tried several methods to coat the substrate to form a defect free polyamide layer. The membranes synthesized in this section were made using the PEI-PIP monomers.

4.4.1 Single polyamide layer

The single polyamide layer formation follows the typical IP procedure whereby the organic phase meets the aqueous phase only once. Figure 27 shows the SEM image of the PTFE substrate with a single layer coating. The polyamide layer was formed on top of smaller pores but failed to cover larger ones. The larger defects were more than 30 μm in length and would render the membrane ineffective for nanofiltration.

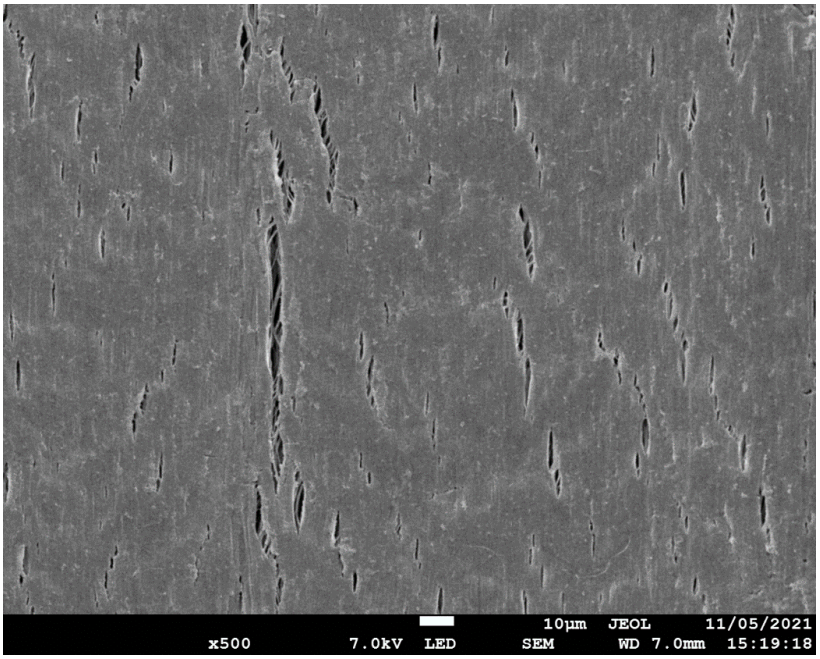

Figure 27 SEM image of substrate with single layer PA coating

There were several attempts to improve the single layer coating. They included:

1. Increasing the concentration of aqueous monomers to increase the IP reaction
2. Increasing concentration and/or circulation time of organic phase reactants to increase the IP reaction
3. Reducing the cyclohexane flush time to ensure more aqueous phase reactant remained in larger pores for subsequent IP reaction

4. Increasing SDS concentration to improve miscibility of aqueous phase in the organic phase reactants since SDS acts as a surfactant
5. Reducing SDS concentration as long carbon chain may hinder with interaction of aqueous and organic monomers
6. Adding IPA to the aqueous solution to reduce interfacial tension
7. Heat treatment of the membrane to increase IP reaction

Despite these attempts, the same problem persisted. The pores of the PTFE substrate were too large and uneven for a defect free layer to be formed in a single IP reaction.

4.4.2 Double polyamide layer

It was thought that the defects after the first IP reaction could acts as ‘pores’ for the subsequent IP reaction. As such after the formation of the single layer, a second round of IP was carried out, whereby the membrane was soaked in the aqueous layer and subjected to another round of TMC again. Figure 28 shows an SEM image of the membrane surface after the second IP reaction.

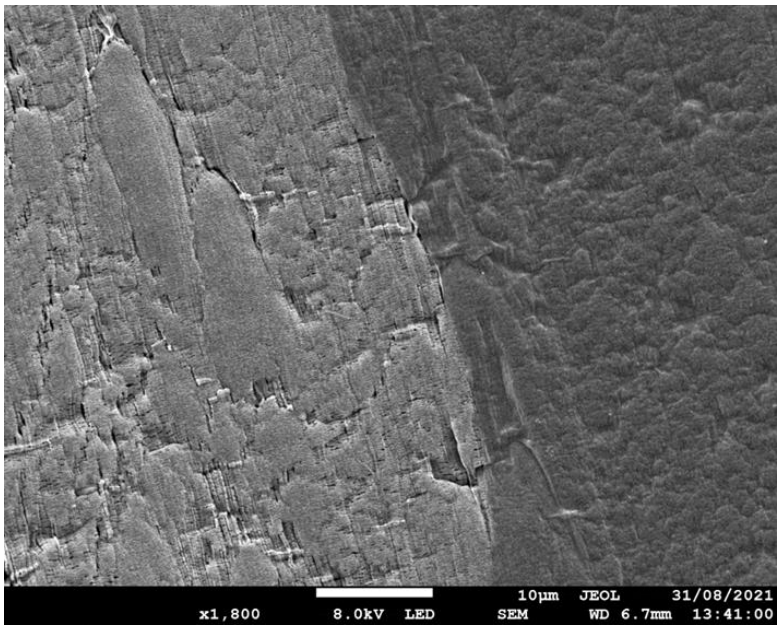

Figure 28 SEM image of delaminated double polyamide layer

Although a defect free PA layer was initially formed, there appeared to be some delamination upon the second round of IP. It is to be noted that most of the surface was well coated and the SEM image only accounts for a small area of the coated

membrane. The substrate appears exposed on one half of the image (lighter part) while the polyamide layer can be clearly seen on the other half (darker part) of the image, suggesting that delamination occurred after the second IP. It is to be noted, however, that the reason for the delamination was unclear. The double layer method was attempted again, this time leaving the membrane to stand for 10 min before the second round of IP. It was hypothesized that the 'rest' time between IP reactions would allow the first layer to fully react and adhere better onto the substrate. The SEM image of the resultant membrane surface can be seen in Figure 29 below.

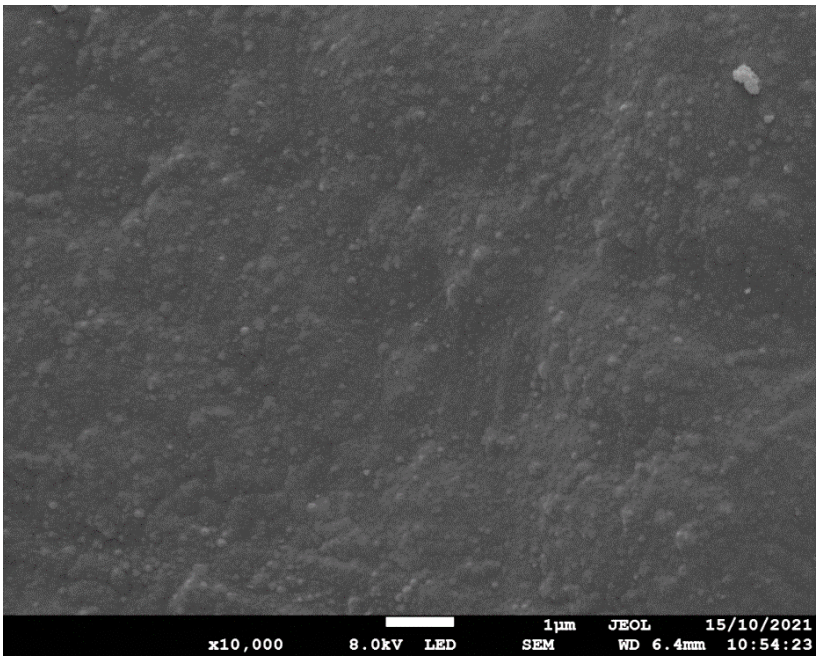

Figure 29 SEM image of successful double polyamide layer

Upon making the changes, a smooth, defect free polyamide layer was formed. However, there were a few concerns. Firstly, the polyamide layer formed was quite thick, thicker than that in Figure 28, and the contours of the underlying substrate cannot be seen, making it not ideal as a selective layer. As a result, the membrane permeability was very low, with a water permeability of only 0.95 $lm^{-2}h^{-1}bar^{-1}$, making it inadequate for commercialization. Secondly, the additional steps required for the double layer formation made the process tedious and time consuming.

4.4.3 Two-time IP method

The two-time IP method was employed in attempts to reduce the thickness of the selective layer and simplify the double PA layer process. As explained in section 2.6, this method consisted of exposing the membrane to the organic phase twice, with heat treatment in between. This process led to a uniform, thin and defect free polyamide layer as seen in Figure 30 below.

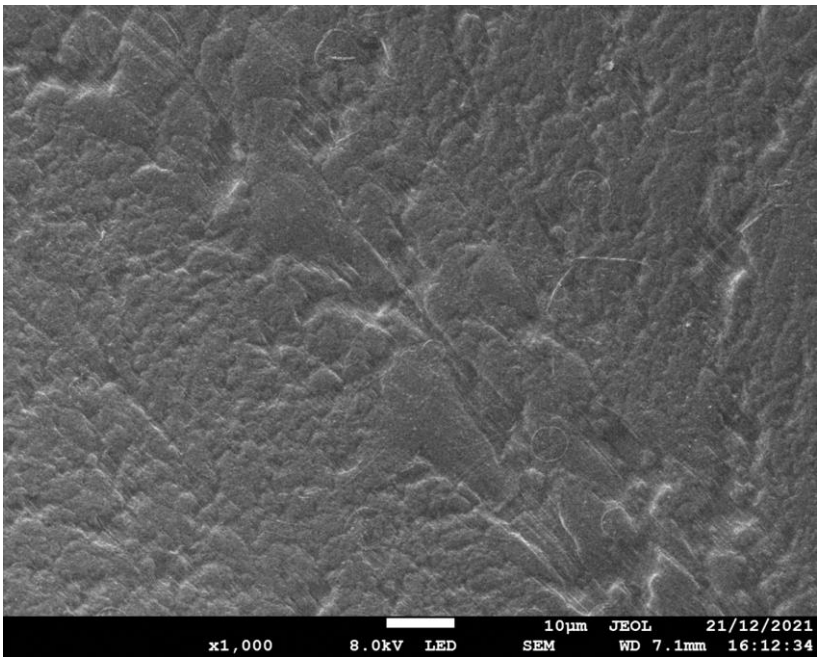

Figure 30 SEM image upon two-time interfacial polymerization

The contours of the underlying substrate could be clearly seen indicating that the formed PA layer was thin and close to the substrate surface. Only PEI was used in the aqueous phase, hence the smooth morphology. One concern was that the two-time IP method would yield a thicker layer. As such the cross section of the membranes from the single layer and two-time IP methods were analyzed as shown in Figure 31.

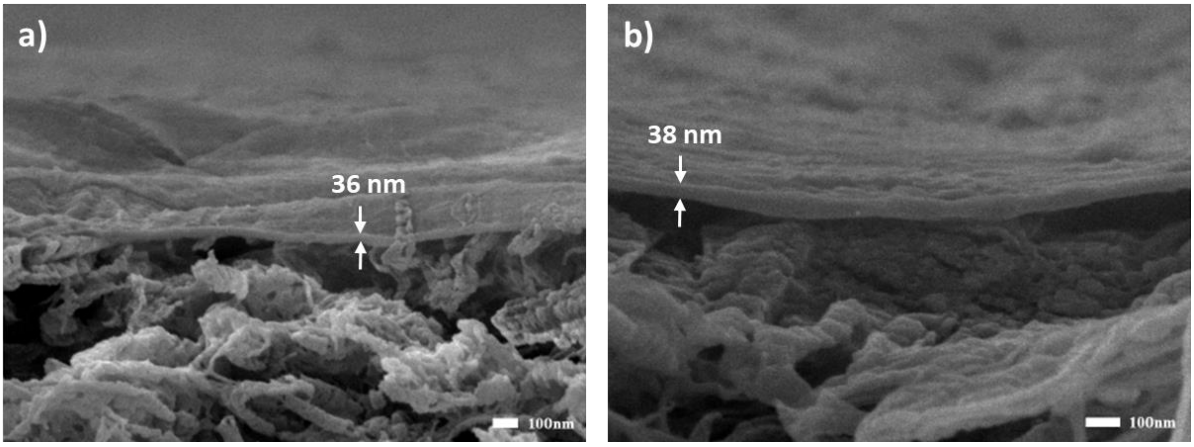

Figure 31 Cross section of membranes using the a) single layer and b) two-time IP methods

It is difficult for PTFE fibres to be cut without affecting the circular geometry of the membrane. Hence, for the cross section to be imaged via SEM, the membranes were first frozen in liquid nitrogen and broken, so that the circular shape of the cross section would not be distorted. The 2nm difference in thickness is negligible, proving that this two-time IP method can be used to improve the polyamide layer formation coating without compromising on its permeability due to a thicker selective layer.

The chemical composition of the membranes was analyzed using FTIR and the full and close-up spectra are as shown in Figure 32. The hollow fibres were cut lengthwise, and the inner surface of the fibres were analyzed. The orange spectrum sows the PTFE substrate while the blue shows the spectrum of the synthesized polyamide-PTFE membrane. For polyamide-PTFE membrane, both the polyamide layer and the PTFE substrate were detected since FTIR is known to have an analysis depth of about a 1 μm [71]. The C-F bond peaks at 1199 and 1145 cm-1 in the wide spectrum (Figure 32a) were large, making the amide peaks very small in comparison. From the close-up spectrum (Figure 32b), the N-H, C=O and NH2 stretches at 1543, 1639 and 2926 cm-1 respectively, are more visible. These peaks correspond to the amide bonds and confirm the formation of the polyamide layer on the PTFE substrate.

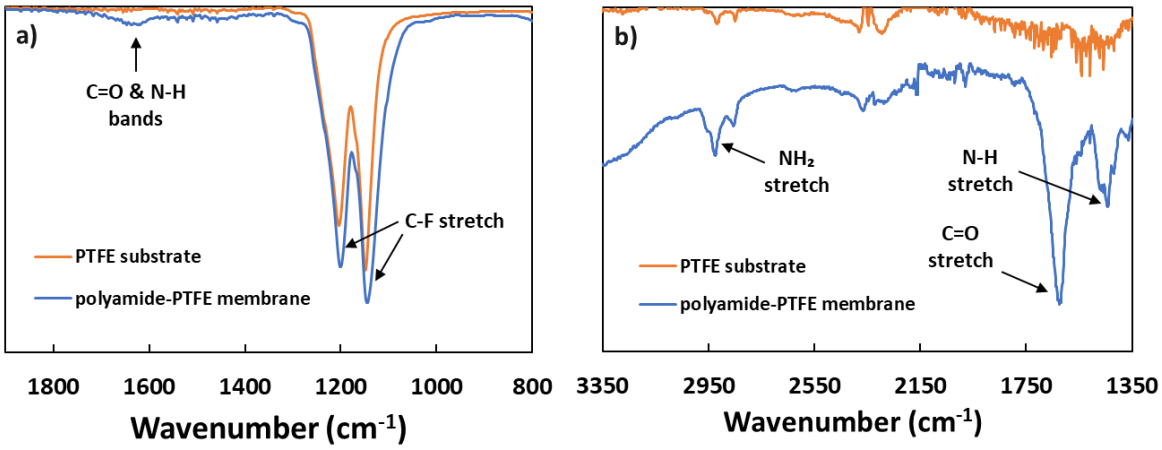

Figure 32 a) Full and b) close-up FTIR spectra

4.5 OSN Performance

It was determined that the PEI-PIP monomers and the two-time coating method were the most suited for creating a thin, defect free polyamide layer on the provided PTFE substrates. As such, this membrane type was further investigated. In section 4.3.1, optimization of the coating formulation was carried out where factors such as monomer concentration, polymerization time and PEI-PIP monomer ratio was studied. The best membrane was then tested on a range of solvents in section 4.3.2, to evaluate its performance. Table 4 shows the various formulations used for the synthesized membranes, which will be further discussed in section 4.3.1.

Table 4 Membrane formulations used

Sample number	PEI (Da)	PIP (wt%)	PIP-PEI ratio	Total concentration of aqueous monomers	TMC (wt%)
M1	0.8k	0	-	0.30	15
M2	70k	0	-	0.30	15
M3	750k	0	-	0.30	15
M4	750k	0	-	0.30	10
M5	750k	0.01	0.03	0.31	15
M6	750k	0.04	0.13	0.34	15

For each sample, 2-3 membranes were synthesized, and the results discussed in the later sections represent the average results of the membranes. Other formulation conditions (concentration of PEI etc.) were kept constant as stated in section 3.2.2.

4.5.1 Optimizing PEI molecular weight

A previous study by Fang et al. showed how the total amine concentration used affects the pure water permeation and rejection properties of the membrane [68]. From that study, it was found that the ideal concentration would be around 0.2-0.3 wt%. Since PEI monomers take up the bulk of the aqueous phase, 0.3 wt% PEI was used in this study.

Varying the PEI molecular weight could vary the ‘porosity’ of the formed polyamide layer, with lower weight monomers forming a tighter polyamide layer. M1, M2 and M3

were synthesized using PEI molecular weights of 0.8k, 70k and 750k Da respectively. The DMF permeability and dye rejection results for AF and MO are shown in Figure 33.

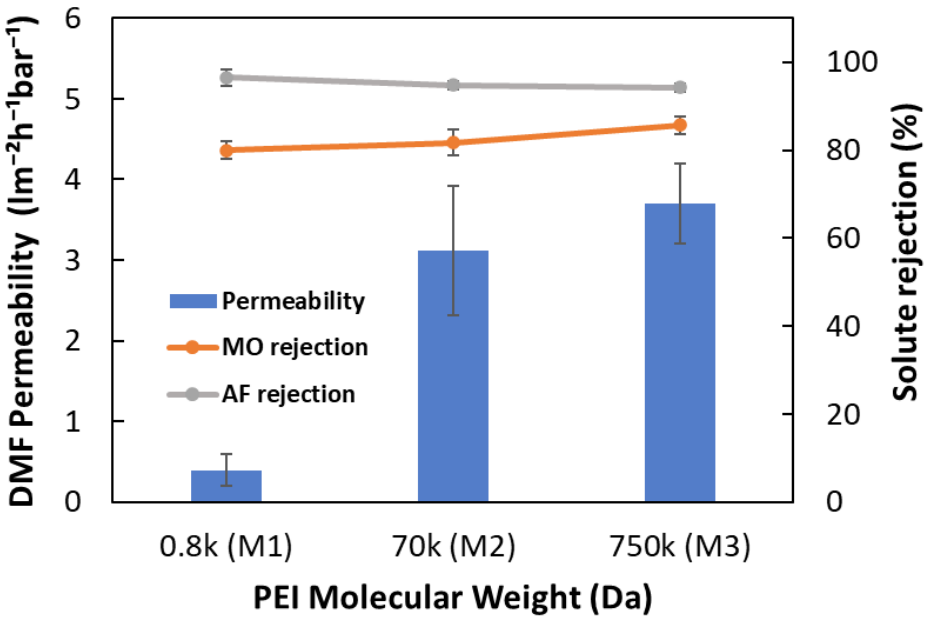

Figure 33 Effects of PEI molecular weight on membrane performance

As expected, the DMF permeability decreased with lower PEI molecular weights with M1 having a permeability of 0.4 $lm^{-2}h^{-1}bar^{-1}$ but M2 and M3 having a permeability of 3.12 and 3.70 $lm^{-2}h^{-1}bar^{-1}$, respectively. Apart from size, the thickness of the polyamide layer could also have played a part in the lower permeability of M1. For the same weight of PEI used (0.3 wt%), there would be more 0.8k Da PEI monomers as compared to that in 70k and 750k Da PEI. The lighter monomer in M1 would also diffuse to the organic-aqueous interface at a faster rate. These factors might have resulted in M1 having a thicker polyamide layer, which could have further reduced its permeability. It should be noted that this increase in selective layer thickness is just a theoretical explanation, and the membrane cross section was not imaged due to the difficulty in the sample preparation.

Apart from forming a looser polyamide layer, the larger PEI monomers tend to be more branched and have more terminal amine groups, making the polyamide layer more positive [72]. This could also explain the slight decrease in rejection for the negatively

charged AF dye as the monomers get larger from M1 to M3. Although the MO rejection trend seems to be the opposite, the results were not precise, as reflected by the larger error margins, and a definitive conclusion cannot be made.

Amongst the membranes synthesized, M2 and M3 showed better performance. As such both the 750 and 70k Da PEI monomers were used in the subsequent sections.

4.5.2 Optimizing TMC concentration

The initial concentration of TMC used was 0.15 wt%. A lower concentration of 0.10 wt% TMC was used for M4, in attempts to reduce the thickness of the polyamide selective layer and increase membrane permeability without affecting its rejection. Figure 34 shows the results from M4 in comparison to that of M3.

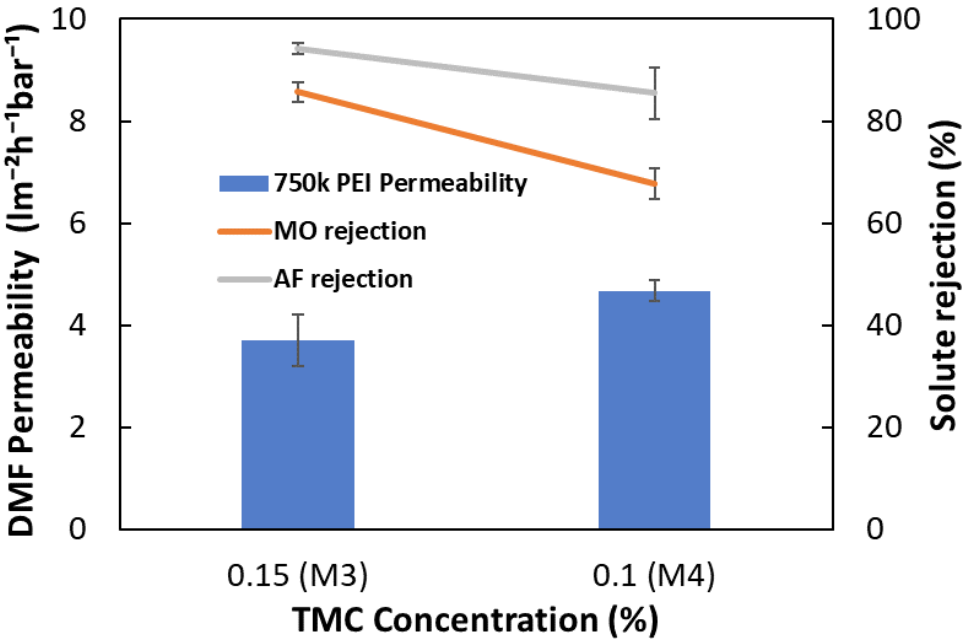

Figure 34 Effect of TMC concentration on membrane performance

There was an increase in DMF permeability that was accompanied with a decrease in dye rejection when a lower concentration of TMC was used in M4. The low AF and MO rejections of 85.5 and 67.8% and the large variation in the rejections indicated that the polyamide layer formed with 0.10 wt% TMC is not complete and stable. There were several samples that broke while testing, confirming this hypothesis. The low TMC concentration may have limited the polymerization, forming a less stable polyamide layer with a lower crosslinking degree.

4.5.3 Optimizing with PIP additives

PIP was then added to the aqueous phase together with the PEI to reduce the MWCO of the membrane. They do this by crosslinking between TMC monomers, reducing the ‘pore size’ in the polyamide matrix as illustrated in Figure 35 below. The area in yellow represents the ‘pores’ in the polyamide network, and it is visibly reduced in size upon addition of PIP.

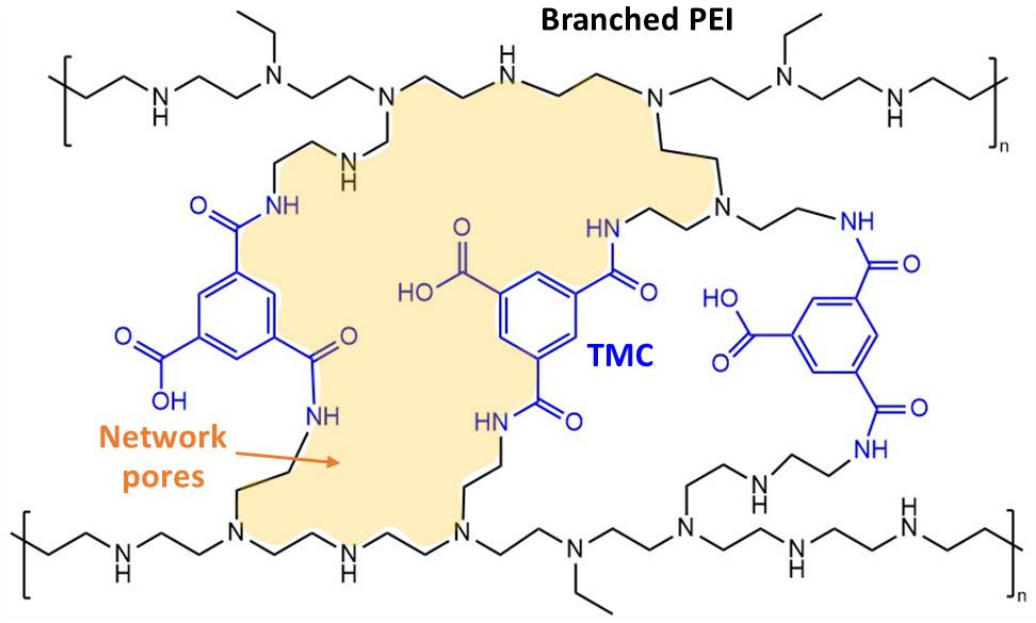

a) Network pores without PIP

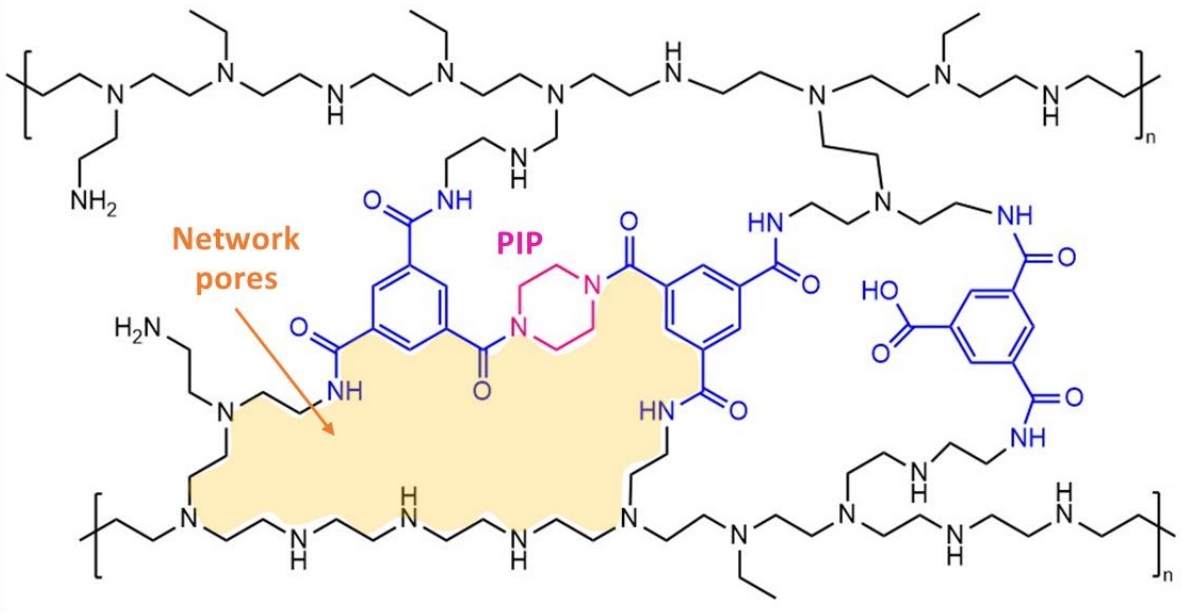

b) Network pores with PIP

Figure 35 Possible chemical structure of polyamide network

Figure 36 shows the results of PIP concentration against DMF permeability for M3, M5 and M6 where 0, 0.01 and 0.04 wt% of PIP was used, respectively. While the AF rejection remained high, the MO rejection improved significantly from 85.7% in M3 to 95.4% in M6. However, the increase in rejection was accompanied by a decrease in rejection as seen from the DMF permeability that dropped by more than 50% from 3.70

to 1.79 $lm^{-2}h^{-1}bar^{-1}$ in M3 and M6, respectively. This decrease in DMF permeability could be due to the tighter polyamide matrix upon the addition of PIP, or the slightly thicker polyamide layer from the higher concentration of aqueous monomers used (Table 1). There was a slight dip in MO rejection from 85.7 to 83.2% in M3 and M5 respectively. Although this drop seems insignificant, some studies have reported a drop in performance for PIP-PEI ratios below 0.1 due to the competing effect between the two aqueous monomers [68, 73]. Having a PIP-PEI ratio of 0.03 (Table 1), this could explain the decline in MO rejection in M3 but the drop in this experiment was too small to conclude for certain that the reduced performance was due to this phenomenon.

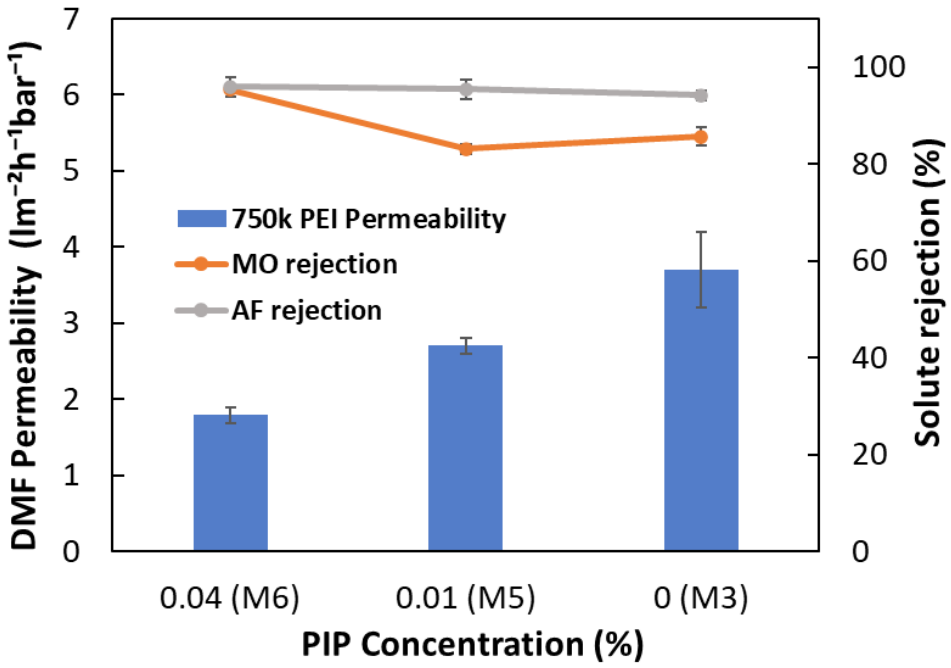

Figure 36 PIP concentration on membrane performance

Figure 37 shows the rejection of M3 and M6 for solutes of varying molecular weights using sudan orange (214 Da), methyl orange (327 Da), acid fuchsin (585 Da) and rose bengal (1017 Da) in DMF. It is difficult to determine the exact MWCO from Figure 37 but it can be seen that M6 had a lower estimated MWCO than M3. It is to be noted that the dyes used are negatively charged and that the rejection values may be lower when a neutral or positively charged dye is used.

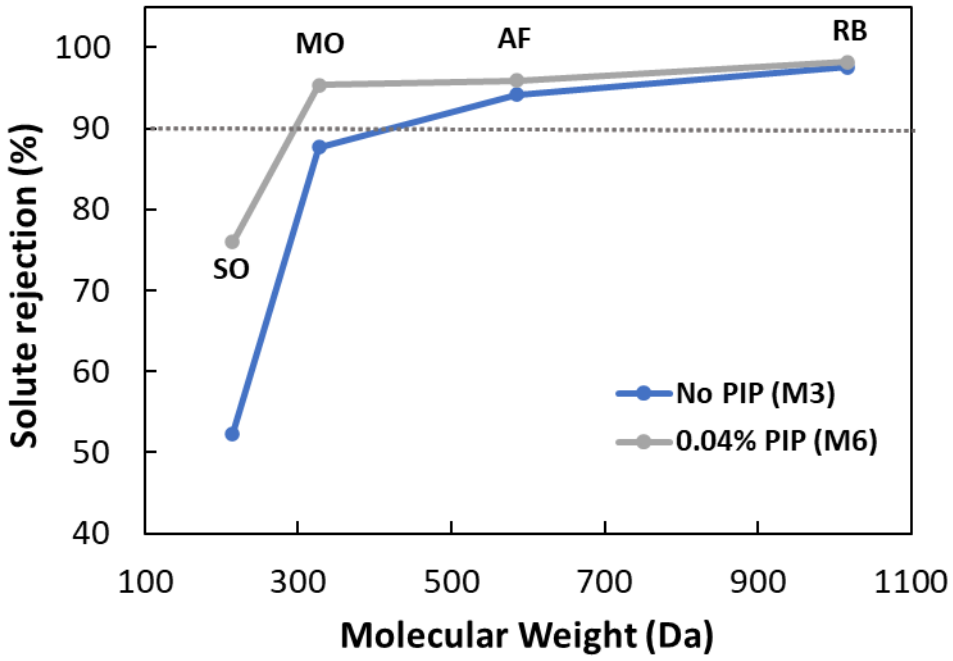

Figure 37 Solute rejection at varying molecular weights

The chemical compositions of M3 and M6 were studied using XPS and the results can be seen in Figure 38. There were two peaks for the C1s spectra. One peak was at 291.8 eV (C-F bonds) and the other was deconvoluted into three peaks: 284.7 eV (C-C and C-H bonds), 285.8 eV (C-N bonds) and 287.7 eV (O-C=O and N-C=O bonds). With an XPS analysis depth of 10 nm at best [57], the C-F peak should not have been detected given that the polyamide layer thickness was around 30-40 nm. One explanation for this would be that the polyamide layer could have cracked during the sample preparation stages of drying and flattening of the hollow fibre. The O1s peak was deconvoluted into two peaks: 531.5 (N-C=O) and 533.0 (O-C=O). From Figure 38c, M6 had a higher N-C=O peak indicating greater crosslinking between the monomers upon the addition of PIP. Apart from confirming the presence of polyamide through FTIR (figure 32), it can also be confirmed through XPS, by the presence of amide bonds (N-C=O) in the deconvoluted C1s and O1s peaks.

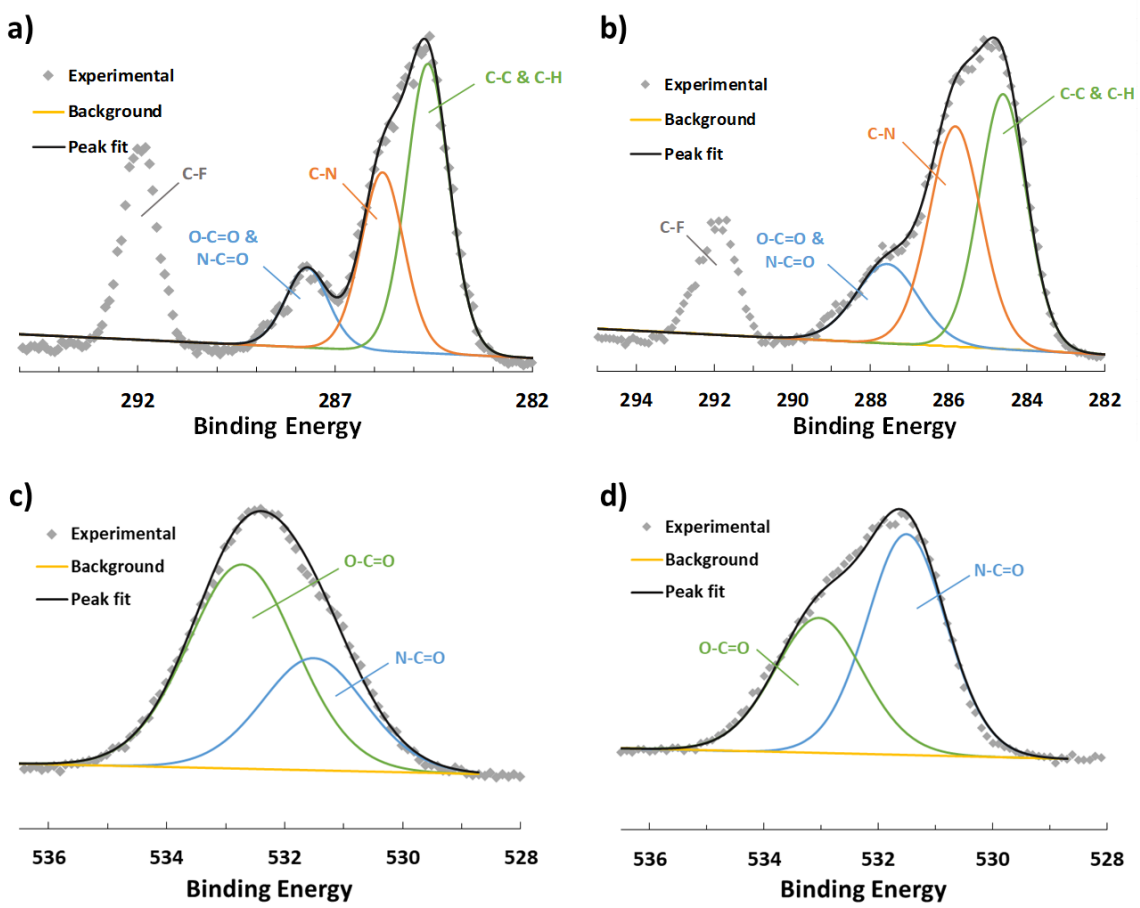

Figure 38 XPS narrow scan spectra of C1s peak of a) M3 and b) M6 and O1s peak of c) M3 and d) M6

The zeta potential results of the PTFE substrate, PDA coated substrate, M3 (no PIP) and M6 (0.04% PIP) are shown in Figure 39. In general, as the pH decreases, the amine groups will get protonated due to the acidic environment and zeta potential increases as a result. The surface of M6 is slightly more negative than that of M3, as seen by its lower isoelectric point. The more negative surface could be due to the PIP increasing the degree of polymerization, leaving fewer unreacted amine groups to be protonated and provide the positive charge [68]. This explanation validates the results obtained from the XPS spectra. The more negative surface of M6 could have also contributed to its higher MO dye rejection. It is possible that the higher negative charge in sample 6 did not increase the AF rejection significantly as it is primarily rejected by size rather than charge.

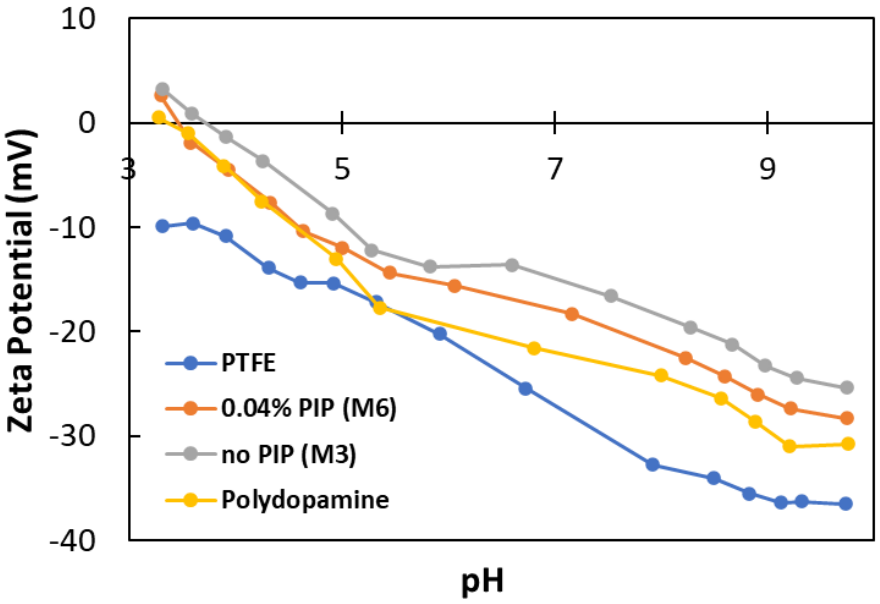

Figure 39 Membrane zeta potential measurement results

4.6 Membrane Stability

The membranes were then tested for their aprotic solvent performance and performance stability over time and when subjected to high pressures. M3 was used for these tests as it showed better performance as compared to the other samples.

4.6.1 Aprotic solvent performance

The performance of the PEI based polyamide-PTFE membrane (M3) was then studied using two other polar aprotic solvents: acetonitrile (ACN) and dimethyl sulfoxide (DMSO). The viscosity and molecular weights of the three solvents used can be seen in table 5.

Table 5 Properties of aprotic solvents used

Solvent	Viscosity (mPas)	Molecular weight (g/mol)
ACN	0.3	41.05
DMF	0.8	73.09
DMSO	2.0	78.13

Figure 40 shows the permeability and dye rejection of the membrane in DMF, ACN, and DMSO. Solvents with a lower viscosity and lower molecular weight will be able to permeate through the membrane faster, explaining the solvent permeability order of ACN>DMF>DMSO [74]. The rejection remained relatively constant, with AF having a rejection of >90% across all three solvents. The minor reduction in AF rejection in DMF and DMSO could be due to the relatively higher solute diffusion rate from their lower permeance. The different swelling degree of the polyamide matrix in different solvents could have also affected the membrane performance. Overall, the high dye rejection proves that the synthesized membranes were stable across a variety of aprotic solvents.

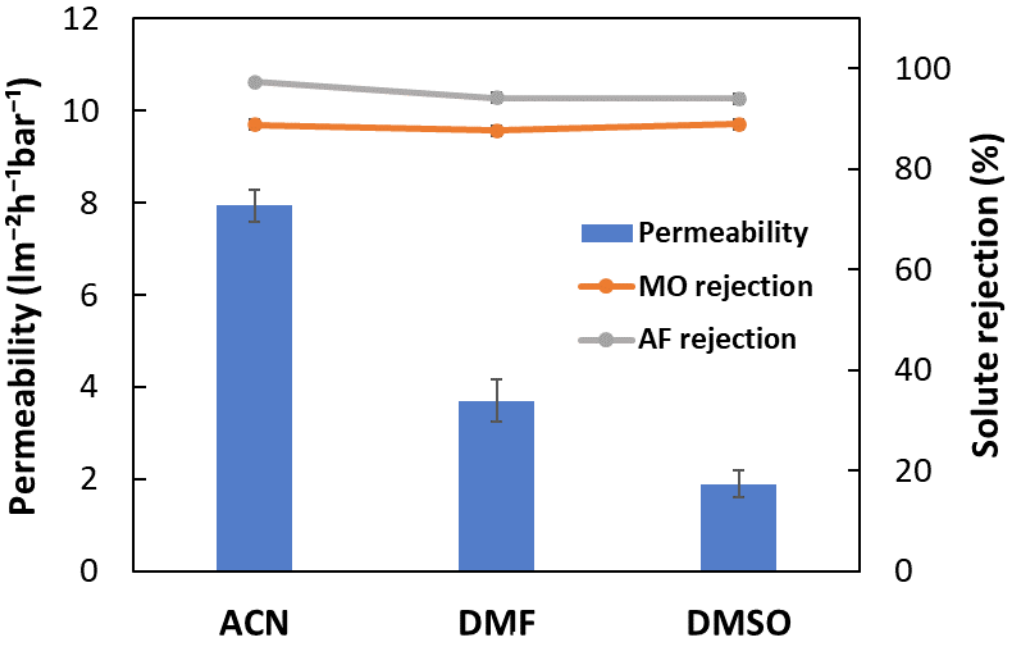

Figure 40 Membrane performance in various aprotic solvents

The performance of the membrane was further analyzed by plotting the permeability of various solvents against $\delta/\eta d^2$, where δ is the solubility parameter, η the solvent viscosity and d the molecular diameter. The results can be seen in Figure 41. The R^2 value of 0.955 shows that the synthesized membrane followed a linear trend, which is expected of polyamide-based membranes [75]. In general, solvents with lower viscosity and smaller molecular diameter would have a higher permeability.

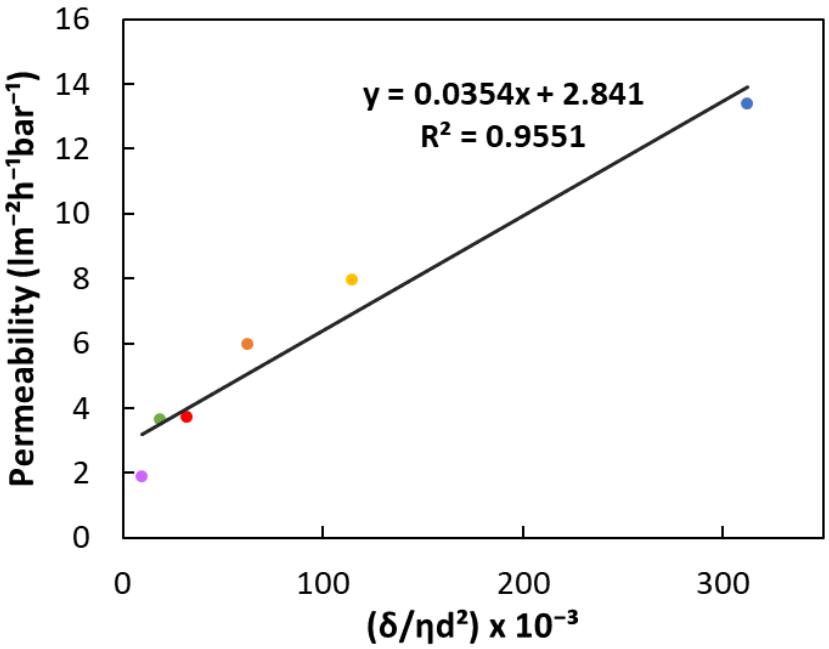

Figure 41 Permeability of various solvents against $\delta/\eta d^2$

4.6.2 Long term and high-pressure performance

To evaluate the membrane's stability over time, a 72-hour DMF permeability test was conducted using 35 μM of AF dye. The set us was left to run overnight prior to sample collection. Samples were collected at 8 h intervals and the results are as shown in Figure 42. The relatively straight line with minimal fluctuations indicated that the membrane performance was stable over the test period, with an average DMF permeability of 2.44 $lm^{-2}h^{-1}bar^{-1}$, and an AF rejection of 93%.

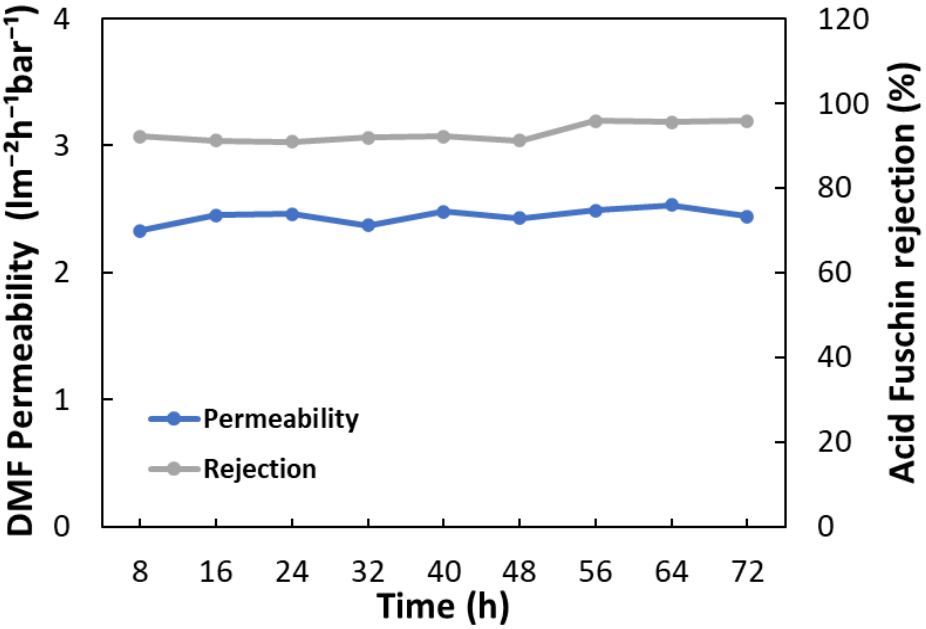

Figure 42 Long term membrane performance

A high-pressure test was also carried out at 5 bar and the results are as seen in Figure 43. During this test period, the polyamide layer could have undergone compaction as indicated by the slight DMF permeability drop from 2.45 to 2.13 $lm^{-2}h^{-1}bar^{-1}$ and increase in AF rejection from 94.2 to 98.5%. Overall, the polyamide-PTFE hollow fibres showed excellent stability over time and under high pressure. They also showed no sign of defect or breakage during the test period.

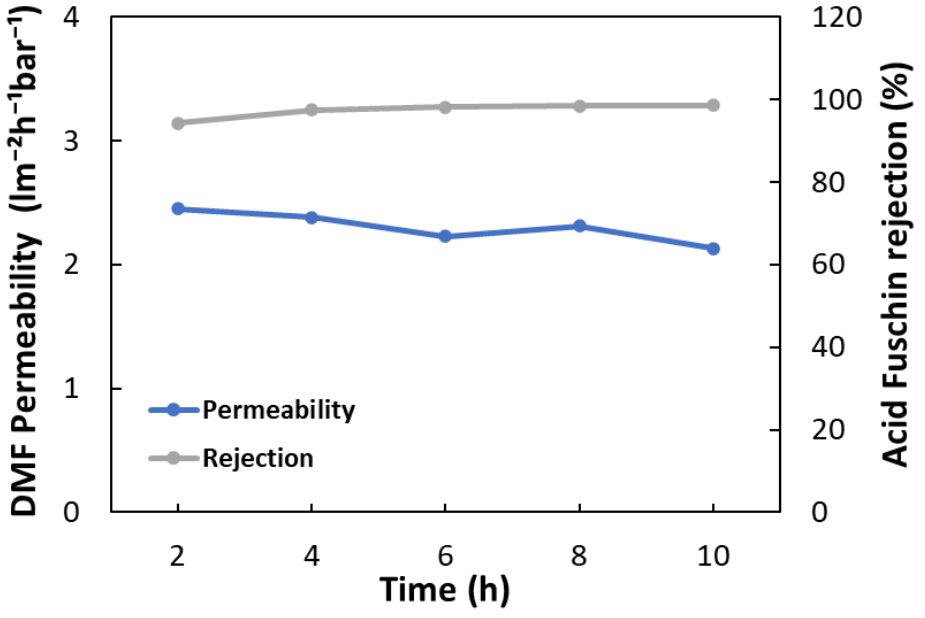

Figure 43 High pressure membrane performance

4.7 Comparison with literature

The performance of the synthesized polyamide-PTFE membrane was then compared with that of other polymeric membranes in literature and is summarized in Table 6 below. Not many OSN membranes have been tested with harsh organic solvents such as DMF and DMSO. The substrates for the flat sheet TFC membrane type required crosslinking for them to be stable in harsh conditions. Their DMF permeability was high, with *7,7'-OH-BINOL/TMC-crosslinked PI* having a permeability of 6.7 $lm^{-2}h^{-1}bar^{-1}$. However, the MWCO of the flat sheet membranes were on the higher side of around 800-1000 Da, with the exception of *PEI/PIP/TMC- imidized PI* which had a MWCO of around 500 Da in DMF.

Minimal research had been done on OSN hollow fibre membranes that can resist strong aprotic solvents. Previous research focused on the ISA type membrane, with this study being the first TFC hollow fibre membrane that can withstand such harsh organic solvents. The DMF permeability of the synthesized polyamide-PTFE membranes were higher than that of previous studies on hollow fibres. In this study, the polyamide layer can be further altered with the addition of PIP to reduce the MWCO from 500 Da to 300 Da. This allows the membranes to be tailored to the specific industrial application.

Table 6 Recent literature on OSN membranes for strong solvents

Type	Membrane (type)	Solvent	DMF permeability ($l\ m^{-2}\ h^{-1}\ bar^{-1}$)	Pressure (bar)	Solute (Mw, Da)	Rejection (%)	Ref. (Year)
Flat Sheet TFC	DAP/TMC-crosslinked PAN	DMF	1.7	15	Brilliant Blue (826)	95	[76] (2015)
					MO (327)	30	
	DAP/TMC-crosslinked PTSC	DMF	5.2	5	RB (1017)	99	[77] (2015)
	MPD/TMC/COF-crosslinked PI	DMF	5.5	10	RB (1017)	99.5	[78] (2019)
	PEI/PIP/TMC- imidized PI	DMF	3.1	4	Janus Green B (511)	98.1	[79] (2021)
	7,7'-OH-BINOL/TMC-crosslinked PI	DMF	6.7	6	RB (1017)	~95	[80] (2021)
Hollow Fibre	Imidized PI (ISA)	DMF	2.5	10	RB (1017)	96.7	[81] (2019)
	Crosslinked PI-BRHF (ISA)	DMF	2.5	15	Chlortetracycline hydrochloride (515)	98	[82] (2021)
	Crosslinked PAI (ISA)	DMF	0.9	2	RB (1017)	98.6	[83] (2016)
	PEEK (ISA)	DMF	2.1	10	Crystal violet (408)	90.7	[84] (2022)
					MO (327)	86.4	
	PEI/TMC-PTFE (TFC)	DMF	3.7	3	AF (585)	94.8	This work
	PEI/PIP/TMC-PTFE (TFC)	DMF	1.79	3	AF (585)	99.9	This work
					MO (327)	95.4	

Abbreviations: TFC: thin film composite, ISA: integrally skinned asymmetric, DAP: diamino piperazine, PAN: polyacrylonitrile, PTSC: polythiosemicarbazide, PAI: polyamide imide, PI: polyimide, PEEK: poly (ether ether ketone), 7.7'-OH-BINOL: 7,7'-dihydroxy-2,20-binaphthol COF: covalent organic framework, BRHF: braid reinforced hollow fibre

5. Future Research

There are four areas that could be further explored: The experimental, analysis, performance tests and industrial applications.

5.1 Experimental: optimizing membrane performance

In this study, the effect of various aqueous monomers on OSN performance was studied. Apart from this, there are various organic monomers that can be used in place of TMC. For instance, 1,2,3,4-cyclobutane tetracarboxylic acid chloride (BTC) had been used in place of TMC in one study [85]. It was found that the BTC-based polyamide layer was denser, thinner and had a higher water permeability than its TMC-based counterpart. However, this study was not conducted using strong solvents and further primary research on this organic monomer is required to form conclusive results.

Although the membranes underwent heat treatment after exposure to TMC, not much research was done on optimizing this process. Both the heating temperature and duration could affect the diffusion of monomers to the surface, the rate of reaction and the resultant polyamide surface morphology [86, 87]. For instance, when the temperature is low, the reaction rate is also slow, allowing the polyamide layer to retain its original molecular structure. However, when the temperature is higher, the molecular motion and reaction rates are increased, leading to different arrangement of the polyamide layer. Optimization of this heat treatment process could lead to better overall membrane performance.

5.2 Analysis: understanding membrane behavior

Further research could be done to better understand the behavior of PDA adhesion and PEI adsorption. Scanning Electron Microscopy with Energy Dispersive X-Ray Analysis (SEM-EDX) could be used to map out the location of PDA and PEI on the substrate surface, giving us a better visual representation of where these molecules are deposited.

To further understand the membrane performance in different solvents, a swelling test could be conducted and calculated using the equation:

$$\text{Degree of swelling (\%)} = \frac{w_w - w_d}{w_w} \times 100 \qquad \text{-(3)}$$

Where *Wd* and *Ww* denote the weight of dry and swollen fiber, respectively [88]. The weight loss of the membrane could also be studied using a similar formula [22]. These results will give an indication on the stability of the membranes in various solvents and if small amounts of the polyamide are being dissolved in the solvents. The results could also help to better explain any anomalies in rejection and/ or permeability.

The membrane behavior can also be further understood through computational membrane modeling and simulations. These simulations can give a better understanding of the transport behavior of various solutes and solvents [89] making it a good direction for further research. These simulations could also be used to predict fouling behavior, a key concern in the industry when implementing membrane technology [90].

5.3 OSN performance tests

Apart from pressure, temperature variations have also shown to affect membrane performance [91-93]. As temperature increases, the permeability and MWCO of the membrane increases. It was also found that tighter membranes were less sensitive to temperature change [93]. Further research on the relationship between temperature and membrane performance would allow for a better understanding of the membrane's use in high temperature feeds.

As mentioned in section 3.4, the dyes used in this study were negatively charged. Since PTFE is also negative, the charges would have played a large role in the rejection results obtained in this study. Hence, more research could be done in using neutral and positively charged dyes to better assess the charge contribution in the rejection results. From this, a better estimate of the MWCO of the membranes could also be obtained.

The aprotic solvents used in this study (ACN, DMF and DMSO) were chosen as they are commonly used solvents in the pharmaceutical industry [49]. Additionally, membrane performance in other commonly used aprotic solvents such as benzene,

toluene, tetrahydrofuran (THF) and N-Methyl-2-pyrrolidone (NMP) could also be studied to get more conclusive data. It should be noted that the above-mentioned solvents are carcinogenic, and care should be taken when handing these chemicals.

5.4 Industrial applications

Lab scale modules cannot provide sufficient information for industrial scale separations due to various factors [94]. As such, further research should be done on the synthesized membranes that were made to target industrial applications. For instance, the IP and coating method in this study should be tested on larger membrane modules with a bigger membrane area to see if a defect free polyamide layer could still be synthesized for large scale industrial purposes. The performance of the membranes at a larger scale should also be evaluated. Waste feeds are also more complex, containing various impurities at high concentrations. The behavior of the synthesized membrane could be different under these conditions and feeds that resemble those in the industry should be used in future research.

6. Conclusion

This study focused on transforming low grade PTFE microfiltration hollow fibre substrates into high value OSN membranes for the filtration of harsh aprotic organic solvents. The PTFE hollow fibres were first surface modified using a simple PDA coating that improved the substrate's hydrophilicity and aided in the retention of the aqueous layer within the substrate pores. The PDA layer was also able to chemically withstand harsh aprotic solvents.

Out of the three aqueous monomers, MPD, PEI and PIP, the PEI/PIP combination was deemed the most suitable due to its lower required monomer concentration and for the ability to tailor the MWCO of the membrane with PIP. The conventional IP process proved to be inadequate in forming a defect free thin polyamide selective layer atop the challenging PTFE substrate. As such, the two-time IP technique was adopted, allowing for a thin, defect free polyamide layer to be synthesized easily atop the large and uneven substrate pores. Optimization of the membrane performance was done by studying the effect of monomer concentration, molecular weight, and PIP-PEI ratio.

The membranes with 750Da PEI and no PIP showed the best performance. With high DMF and DMSO permeabilities of 3.70 $lm^{-2}h^{-1}bar^{-1}$ and 1.89 $lm^{-2}h^{-1}bar^{-1}$ respectively, these membranes show potential for commercial applications such as in active pharmaceutical ingredient (API) purification and food additive synthesis, and solvent recovery [95]. When 0.04 wt% PIP was added, the MWCO of the membrane reduced from 585 Da to 327 Da, indicating that the polyamide-PTFE membranes can be tailored for their intended use, through the incorporation of PIP monomers into the aqueous phase. This is the first study to successfully show that PTFE hollow fibres can be used in the OSN of harsh, polar aprotic solvents.

References

[1] R.W. A.G. (Tony) Fane, and Yue Jia, Membrane and Desalination Technologies, Humana Press2011.
[2] I. Soroko, M.P. Lopes, A. Livingston, The effect of membrane formation parameters on performance of polyimide membranes for organic solvent nanofiltration (OSN): Part A. Effect of polymer/solvent/non-solvent system choice, Journal of Membrane Science 381(1-2) (2011) 152-162. https://doi.org/10.1016/j.memsci.2011.07.027.
[3] W. Chen, C. Qian, K.-G. Zhou, H.-Q. Yu, Molecular Spectroscopic Characterization of Membrane Fouling: A Critical Review, Chem 4(7) (2018) 1492-1509. https://doi.org/10.1016/j.chempr.2018.03.011.
[4] S. Darvishmanesh, L. Firoozpour, J. Vanneste, P. Luis, J. Degrève, B.V.d. Bruggen, Performance of solvent resistant nanofiltration membranes for purification of residual solvent in the pharmaceutical industry: experiments and simulation, Green Chemistry 13(12) (2011). https://doi.org/10.1039/c1gc15462a.
[5] L. Peeva, J.d.S. Burgal, I. Valtcheva, A.G. Livingston, Continuous purification of active pharmaceutical ingredients using multistage organic solvent nanofiltration membrane cascade, Chemical Engineering Science 116 (2014) 183-194. https://doi.org/10.1016/j.ces.2014.04.022.
[6] M.G. Buonomenna, J. Bae, Organic Solvent Nanofiltration in Pharmaceutical Industry, Separation & Purification Reviews 44(2) (2014) 157-182. https://doi.org/10.1080/15422119.2014.918884.
[7] A.A. Kiss, Distillation technology - still young and full of breakthrough opportunities, Journal of Chemical Technology & Biotechnology 89(4) (2014) 479-498. https://doi.org/10.1002/jctb.4262.
[8] G.M. Geise, H.-S. Lee, D.J. Miller, B.D. Freeman, J.E. McGrath, D.R. Paul, Water purification by membranes: The role of polymer science, Journal of Polymer Science Part B: Polymer Physics 48(15) (2010) 1685-1718. https://doi.org/10.1002/polb.22037.
[9] Y. Lu, Z. Wang, W. Fang, Y. Zhu, Y. Zhang, J. Jin, Polyamide Thin Films Grown on PD/SWCNT-Interlayered-PTFE Microfiltration Membranes for High-Permeance Organic Solvent Nanofiltration, Industrial & Engineering Chemistry Research 59(52) (2020) 22533-22540. https://doi.org/10.1021/acs.iecr.0c04969.
[10] Z. Zhou, Y. Ying, X. Peng, High efficient thin-film composite membrane: Ultrathin hydrophilic polyamide film on macroporous superhydrophobic polytetrafluoroethylene substrate, Applied Materials Today 8 (2017) 54-59. https://doi.org/10.1016/j.apmt.2017.04.002.
[11] Z. Yang, Z.W. Zhou, H. Guo, Z. Yao, X.H. Ma, X. Song, S.P. Feng, C.Y. Tang, Tannic Acid/Fe(3+) Nanoscaffold for Interfacial Polymerization: Toward Enhanced Nanofiltration Performance, Environ Sci Technol 52(16) (2018) 9341-9349. https://doi.org/10.1021/acs.est.8b02425.
[12] P. Vandezande, L.E. Gevers, I.F. Vankelecom, Solvent resistant nanofiltration: separating on a molecular level, Chem Soc Rev 37(2) (2008) 365-405. https://doi.org/10.1039/b610848m.
[13] S. Lee, T. Kang, J.Y. Lee, J. Park, S.H. Choi, J.Y. Yu, S. Ok, S.H. Park, Thin-Film Composite Nanofiltration Membranes for Non-Polar Solvents, Membranes (Basel) 11(3) (2021). https://doi.org/10.3390/membranes11030184.
[14] P. Marchetti, M.F. Jimenez Solomon, G. Szekely, A.G. Livingston, Molecular separation with organic solvent nanofiltration: a critical review, Chem Rev 114(21) (2014) 10735-806. https://doi.org/10.1021/cr500006j.
[15] S. Feng, Z. Zhong, Y. Wang, W. Xing, E. Drioli, Progress and perspectives in PTFE membrane: Preparation, modification, and applications, Journal of Membrane Science 549 (2018) 332-349. https://doi.org/10.1016/j.memsci.2017.12.032.
[16] H. Wang, S. Ding, H. Zhu, F. Wang, Y. Guo, H. Zhang, J. Chen, Effect of stretching ratio and heating temperature on structure and performance of PTFE hollow fiber membrane in VMD for RO brine, Separation and Purification Technology 126 (2014) 82-94. https://doi.org/10.1016/j.seppur.2014.02.027.

[17] J. Hashisho, M. El-Fadel, M. Al-Hindi, D. Salam, I. Alameddine, Hollow fiber vs. flat sheet MBR for the treatment of high strength stabilized landfill leachate, Waste Management 55 (2016) 249-256. https://doi.org/10.1016/j.wasman.2015.12.016.
[18] S.A. Rackley, Membrane separation systems, Carbon Capture and Storage2017, pp. 187-225. https://doi.org/10.1016/b978-0-12-812041-5.00008-8.
[19] L.W. McKeen, Markets and Applications for Films, Containers, and Membranes, Permeability Properties of Plastics and Elastomers2012, pp. 59-75. https://doi.org/10.1016/b978-1-4377-3469-0.10004-9.
[20] J.Y. Chong, R. Wang, From micro to nano: Polyamide thin film on microfiltration ceramic tubular membranes for nanofiltration, Journal of Membrane Science 587 (2019). https://doi.org/10.1016/j.memsci.2019.06.001.
[21] A. Lee, J.W. Elam, S.B. Darling, Membrane materials for water purification: design, development, and application, Environmental Science: Water Research & Technology 2(1) (2016) 17-42. https://doi.org/10.1039/c5ew00159e.
[22] K.S. Goh, J.Y. Chong, Y. Chen, W. Fang, T.-H. Bae, R. Wang, Thin-film composite hollow fibre membrane for low pressure organic solvent nanofiltration, Journal of Membrane Science 597 (2020). https://doi.org/10.1016/j.memsci.2019.117760.
[23] C.F. Wan, T. Yang, W. Gai, Y.D. Lee, T.-S. Chung, Thin-film composite hollow fiber membrane with inorganic salt additives for high mechanical strength and high power density for pressure-retarded osmosis, Journal of Membrane Science 555 (2018) 388-397. https://doi.org/10.1016/j.memsci.2018.03.050.
[24] Y. Tang, N. Li, A. Liu, S. Ding, C. Yi, H. Liu, Effect of spinning conditions on the structure and performance of hydrophobic PVDF hollow fiber membranes for membrane distillation, Desalination 287 (2012) 326-339. https://doi.org/10.1016/j.desal.2011.11.045.
[25] T. Zhu, Q. Xia, J. Zuo, S. Liu, X. Yu, Y. Wang, Recent advances of thin film composite membranes for pervaporation applications: A comprehensive review, Advanced Membranes 1 (2021). https://doi.org/10.1016/j.advmem.2021.100008.
[26] L. Xia, J.R. McCutcheon, Understanding the influence of solvents on the intrinsic properties and performance of polyamide thin film composite membranes, Separation and Purification Technology 238 (2020). https://doi.org/10.1016/j.seppur.2019.116398.
[27] L. Xia, J. Ren, M. Weyd, J.R. McCutcheon, Ceramic-supported thin film composite membrane for organic solvent nanofiltration, Journal of Membrane Science 563 (2018) 857-863. https://doi.org/10.1016/j.memsci.2018.05.069.
[28] I. Soroko, Y. Bhole, A.G. Livingston, Environmentally friendly route for the preparation of solvent resistant polyimide nanofiltration membranes, Green Chem. 13(1) (2011) 162-168. https://doi.org/10.1039/c0gc00155d.
[29] D. Aryal, V. Ganesan, Impact of cross-linking of polymers on transport of salt and water in polyelectrolyte membranes: A mesoscopic simulation study, J Chem Phys 149(22) (2018) 224902. https://doi.org/10.1063/1.5057708.
[30] K. Vanherck, G. Koeckelberghs, I.F.J. Vankelecom, Crosslinking polyimides for membrane applications: A review, Progress in Polymer Science 38(6) (2013) 874-896. https://doi.org/10.1016/j.progpolymsci.2012.11.001.
[31] K. Vanherck, P. Vandezande, S.O. Aldea, I.F.J. Vankelecom, Cross-linked polyimide membranes for solvent resistant nanofiltration in aprotic solvents, Journal of Membrane Science 320(1-2) (2008) 468-476. https://doi.org/10.1016/j.memsci.2008.04.026.
[32] S. Xu, L. Liu, Y. Wang, Network cross-linking of polyimide membranes for pervaporation dehydration, Separation and Purification Technology 185 (2017) 215-226. https://doi.org/10.1016/j.seppur.2017.05.037.
[33] M.J.T. Raaijmakers, N.E. Benes, Current trends in interfacial polymerization chemistry, Progress in Polymer Science 63 (2016) 86-142. https://doi.org/10.1016/j.progpolymsci.2016.06.004.

[34] C. Perignon, G. Ongmayeb, R. Neufeld, Y. Frere, D. Poncelet, Microencapsulation by interfacial polymerisation: membrane formation and structure, J Microencapsul 32(1) (2015) 1-15. https://doi.org/10.3109/02652048.2014.950711.
[35] J. Jegal, S.G. Min, K.-H. Lee, Factors affecting the interfacial polymerization of polyamide active layers for the formation of polyamide composite membranes, Journal of Applied Polymer Science 86(11) (2002) 2781-2787. https://doi.org/10.1002/app.11257.
[36] M.F. Jimenez-Solomon, P. Gorgojo, M. Munoz-Ibanez, A.G. Livingston, Beneath the surface: Influence of supports on thin film composite membranes by interfacial polymerization for organic solvent nanofiltration, Journal of Membrane Science 448 (2013) 102-113. https://doi.org/10.1016/j.memsci.2013.06.030.
[37] A.F.M. Alsayed, M.A. Ashraf, Modified nanofiltration membrane treatment of saline water, Water Engineering Modeling and Mathematic Tools2021, pp. 25-44. https://doi.org/10.1016/b978-0-12-820644-7.00005-0.
[38] Y.J. Lim, K. Goh, M. Kurihara, R. Wang, Seawater desalination by reverse osmosis: Current development and future challenges in membrane fabrication – A review, Journal of Membrane Science 629 (2021). https://doi.org/10.1016/j.memsci.2021.119292.
[39] C. Liu, Y. Guo, J. Zhang, B. Tian, O. Lin, Y. Liu, C. Zhang, Tailor-made high-performance reverse osmosis membranes by surface fixation of hydrophilic macromolecules for wastewater treatment, RSC Adv 9(31) (2019) 17766-17777. https://doi.org/10.1039/c9ra02240f.
[40] L. Upadhyaya, X. Qian, S. Ranil Wickramasinghe, Chemical modification of membrane surface — overview, Current Opinion in Chemical Engineering 20 (2018) 13-18. https://doi.org/10.1016/j.coche.2018.01.002.
[41] S. Turmanova, M. Minchev, K. Vassilev, G. Danev, Surface grafting polymerization of vinyl monomers on poly(tetrafluoroethylene) films by plasma treatment, Journal of Polymer Research 15(4) (2008) 309-318. https://doi.org/10.1007/s10965-007-9172-0.
[42] H. Song, H. Yu, L. Zhu, L. Xue, D. Wu, H. Chen, Durable hydrophilic surface modification for PTFE hollow fiber membranes, Reactive and Functional Polymers 114 (2017) 110-117. https://doi.org/10.1016/j.reactfunctpolym.2017.03.010.
[43] S.M.D. Haeshin Lee, William M. Miller, Phillip B. Messersmith, Mussel-Inspired Surface Chemistry for Multifunctional Coatings, Science 318(5849) (2007) 426-430.
[44] C. Zhang, Y. Ou, W.X. Lei, L.S. Wan, J. Ji, Z.K. Xu, CuSO4/H2O2-Induced Rapid Deposition of Polydopamine Coatings with High Uniformity and Enhanced Stability, Angew Chem Int Ed Engl 55(9) (2016) 3054-7. https://doi.org/10.1002/anie.201510724.
[45] R. Dai, J. Li, Z. Wang, Constructing interlayer to tailor structure and performance of thin-film composite polyamide membranes: A review, Adv Colloid Interface Sci 282 (2020) 102204. https://doi.org/10.1016/j.cis.2020.102204.
[46] W. Yang, H. Xu, W. Chen, Z. Shen, M. Ding, T. Lin, H. Tao, Q. Kong, G. Yang, Z. Xie, A polyamide membrane with tubular crumples incorporating carboxylated single-walled carbon nanotubes for high water flux, Desalination 479 (2020). https://doi.org/10.1016/j.desal.2020.114330.
[47] C. Ji, Z. Zhai, C. Jiang, P. Hu, S. Zhao, S. Xue, Z. Yang, T. He, Q.J. Niu, Recent advances in high-performance TFC membranes: A review of the functional interlayers, Desalination 500 (2021). https://doi.org/10.1016/j.desal.2020.114869.
[48] K. Chen, P. Li, H. Zhang, H. Sun, X. Yang, D. Yao, X. Pang, X. Han, Q. Jason Niu, Organic solvent nanofiltration membrane with improved permeability by in-situ growth of metal-organic frameworks interlayer on the surface of polyimide substrate, Separation and Purification Technology 251 (2020). https://doi.org/10.1016/j.seppur.2020.117387.
[49] J. Chau, K.K. Sirkar, K.J. Pennisi, G. Vaseghi, L. Derdour, B. Cohen, Novel perfluorinated nanofiltration membranes for isolation of pharmaceutical compounds, Separation and Purification Technology 258 (2021). https://doi.org/10.1016/j.seppur.2020.117944.

[50] Y. Feng, T. Xiong, S. Jiang, S. Liu, H. Hou, Mechanical properties and chemical resistance of electrospun polyterafluoroethylene fibres, RSC Advances 6(29) (2016) 24250-24256. https://doi.org/10.1039/c5ra27676d.
[51] L.-T. Huang, P.-S. Hsu, C.-Y. Kuo, S.-C. Chen, J.-Y. Lai, Pore size control of PTFE membranes by stretch operation with asymmetric heating system, Desalination 233(1-3) (2008) 64-72. https://doi.org/10.1016/j.desal.2007.09.028.
[52] Y. Zong, R. Zhang, S. Gao, H. Chang, B. Van der Bruggen, J. Tian, Anti-drying nanofiltration (NF) membranes constructed on PTFE microfiltration (MF) substrate via novel interfacial polymerization, Journal of Membrane Science 638 (2021). https://doi.org/10.1016/j.memsci.2021.119721.
[53] B.J. Inkson, Scanning electron microscopy (SEM) and transmission electron microscopy (TEM) for materials characterization, Materials Characterization Using Nondestructive Evaluation (NDE) Methods2016, pp. 17-43. https://doi.org/10.1016/b978-0-08-100040-3.00002-x.
[54] E.-S. Jang, C.-W. Kang, The pore structure and sound absorption capabilities of Homalium (Homalium foetidum) and Jelutong (Dyera costulata), Wood Science and Technology 56(1) (2021) 323-344. https://doi.org/10.1007/s00226-021-01336-z.
[55] B.E. Rapp, Surface Tension, Microfluidics: Modelling, Mechanics and Mathematics2017, pp. 421-444. https://doi.org/10.1016/b978-1-4557-3141-1.50020-4.
[56] S. Semenov, V. Starov, R.G. Rubio, Droplets with Surfactants, Droplet Wetting and Evaporation2015, pp. 315-337. https://doi.org/10.1016/b978-0-12-800722-8.00021-7.
[57] M.H. Engelhard, T.C. Droubay, Y. Du, X-Ray Photoelectron Spectroscopy Applications, Encyclopedia of Spectroscopy and Spectrometry2017, pp. 716-724. https://doi.org/10.1016/b978-0-12-409547-2.12102-x.
[58] H. Seyama, M. Soma, B.K.G. Theng, X-Ray Photoelectron Spectroscopy, Handbook of Clay Science2013, pp. 161-176. https://doi.org/10.1016/b978-0-08-098259-5.00007-x.
[59] S.-J. Park, M.-K. Seo, Intermolecular Force, Interface Science and Composites2011, pp. 1-57. https://doi.org/10.1016/b978-0-12-375049-5.00001-3.
[60] P. Fievet, A. Szymczyk, C. Labbez, B. Aoubiza, C. Simon, A. Foissy, J. Pagetti, Determining the Zeta Potential of Porous Membranes Using Electrolyte Conductivity inside Pores, J Colloid Interface Sci 235(2) (2001) 383-390. https://doi.org/10.1006/jcis.2000.7331.
[61] D.L. Oatley-Radcliffe, N. Aljohani, P.M. Williams, N. Hilal, Electrokinetic Phenomena for Membrane Charge, Membrane Characterization2017, pp. 405-422. https://doi.org/10.1016/b978-0-444-63776-5.00018-8.
[62] D.F. Swinehart, The Beer-Lambert Law, 39 (1962) 333-335.
[63] E.I. Alarcon, H. Poblete, H. Roh, J.F. Couture, J. Comer, I.E. Kochevar, Rose Bengal Binding to Collagen and Tissue Photobonding, ACS Omega 2(10) (2017) 6646-6657. https://doi.org/10.1021/acsomega.7b00675.
[64] J. Mun, H.M. Park, E. Koh, Y.T. Lee, Enhancement of the crystallinity and surface hydrophilicity of a PVDF hollow fiber membrane on simultaneous stretching and coating method, Journal of Industrial and Engineering Chemistry 65 (2018) 112-119. https://doi.org/10.1016/j.jiec.2018.04.019.
[65] J.-G. Park, S.-H. Lee, J.-S. Ryu, Y.-K. Hong, T.-G. Kim, A.A. Busnaina, Interfacial and Electrokinetic Characterization of IPA Solutions Related to Semiconductor Wafer Drying and Cleaning, Journal of The Electrochemical Society 153(9) (2006). https://doi.org/10.1149/1.2214532.
[66] X. Jiang, Y. Wang, M. Li, Selecting water-alcohol mixed solvent for synthesis of polydopamine nano-spheres using solubility parameter, Sci Rep 4 (2014) 6070. https://doi.org/10.1038/srep06070.
[67] D. Wu, S. Yu, D. Lawless, X. Feng, Thin film composite nanofiltration membranes fabricated from polymeric amine polyethylenimine imbedded with monomeric amine piperazine for enhanced salt separations, Reactive and Functional Polymers 86 (2015) 168-183. https://doi.org/10.1016/j.reactfunctpolym.2014.08.009.
[68] W. Fang, L. Shi, R. Wang, Mixed polyamide-based composite nanofiltration hollow fiber membranes with improved low-pressure water softening capability, Journal of Membrane Science 468 (2014) 52-61. https://doi.org/10.1016/j.memsci.2014.05.047.

[69] M.F. Hamid, N. Abdullah, N. Yusof, N.M. Ismail, A.F. Ismail, W.N.W. Salleh, J. Jaafar, F. Aziz, W.J. Lau, Effects of surface charge of thin-film composite membrane on copper (II) ion removal by using nanofiltration and forward osmosis process, Journal of Water Process Engineering 33 (2020). https://doi.org/10.1016/j.jwpe.2019.101032.
[70] Z. Zhou, D. Lu, X. Li, L.M. Rehman, A. Roy, Z. Lai, Fabrication of highly permeable polyamide membranes with large "leaf-like" surface nanostructures on inorganic supports for organic solvent nanofiltration, Journal of Membrane Science 601 (2020). https://doi.org/10.1016/j.memsci.2020.117932.
[71] S. Eibl, Observing Inhomogeneity of Plastic Components in Carbon Fiber Reinforced Polymer Materials by ATR-FTIR Spectroscopy in the Micrometer Scale, Journal of Composite Materials 42(12) (2008) 1231-1246. https://doi.org/10.1177/0021998308091734.
[72] W. Fang, L. Shi, R. Wang, Interfacially polymerized composite nanofiltration hollow fiber membranes for low-pressure water softening, Journal of Membrane Science 430 (2013) 129-139. https://doi.org/10.1016/j.memsci.2012.12.011.
[73] N.K. Saha, S.V. Joshi, Performance evaluation of thin film composite polyamide nanofiltration membrane with variation in monomer type, Journal of Membrane Science 342(1-2) (2009) 60-69. https://doi.org/10.1016/j.memsci.2009.06.025.
[74] S. Ilyas, N. Joseph, A. Szymczyk, A. Volodin, K. Nijmeijer, W.M. de Vos, I.F.J. Vankelecom, Weak polyelectrolyte multilayers as tunable membranes for solvent resistant nanofiltration, Journal of Membrane Science 514 (2016) 322-331. https://doi.org/10.1016/j.memsci.2016.04.073.
[75] D.B. Shinde, G. Sheng, X. Li, M. Ostwal, A.H. Emwas, K.W. Huang, Z. Lai, Crystalline 2D Covalent Organic Framework Membranes for High-Flux Organic Solvent Nanofiltration, J Am Chem Soc 140(43) (2018) 14342-14349. https://doi.org/10.1021/jacs.8b08788.
[76] L. Pérez-Manríquez, J. Aburabi'e, P. Neelakanda, K.-V. Peinemann, Cross-linked PAN-based thin-film composite membranes for non-aqueous nanofiltration, Reactive and Functional Polymers 86 (2015) 243-247. https://doi.org/10.1016/j.reactfunctpolym.2014.09.015.
[77] J. Aburabie, P. Neelakanda, M. Karunakaran, K.-V. Peinemann, Thin-film composite crosslinked polythiosemicarbazide membranes for organic solvent nanofiltration (OSN), Reactive and Functional Polymers 86 (2015) 225-232. https://doi.org/10.1016/j.reactfunctpolym.2014.09.011.
[78] C. Li, S. Li, L. Tian, J. Zhang, B. Su, M.Z. Hu, Covalent organic frameworks (COFs)-incorporated thin film nanocomposite (TFN) membranes for high-flux organic solvent nanofiltration (OSN), Journal of Membrane Science 572 (2019) 520-531. https://doi.org/10.1016/j.memsci.2018.11.005.
[79] T.-D. Lu, L.-L. Zhao, W.F. Yong, Q. Wang, L. Duan, S.-P. Sun, Highly solvent-durable thin-film molecular sieve membranes with insoluble polyimide nanofibrous substrate, Chemical Engineering Journal 409 (2021). https://doi.org/10.1016/j.cej.2020.128206.
[80] W. Fu, W. Zhang, H. Chen, S.-L. Li, W. Shi, Y. Hu, A high-flux organic solvent nanofiltration membrane with binaphthol-based rigid-flexible microporous structures, Journal of Materials Chemistry A 9(11) (2021) 7180-7189. https://doi.org/10.1039/d0ta10632a.
[81] Y. Li, B. Cao, P. Li, Effects of dope compositions on morphologies and separation performances of PMDA-ODA polyimide hollow fiber membranes in aqueous and organic solvent systems, Applied Surface Science 473 (2019) 1038-1048. https://doi.org/10.1016/j.apsusc.2018.12.245.
[82] Z.-Y. Wang, R. Feng, W.-J. Wang, Y.-X. Sun, S.-N. Tao, Y.-M. Wang, Y.-F. Chen, Z.-J. Fu, X.-L. Cao, S.-P. Sun, W. Xing, Robust braid reinforced hollow fiber membranes for organic solvent nanofiltration (OSN), Advanced Membranes 1 (2021). https://doi.org/10.1016/j.advmem.2021.100007.
[83] S.K. Lim, L. Setiawan, T.-H. Bae, R. Wang, Polyamide-imide hollow fiber membranes crosslinked with amine-appended inorganic networks for application in solvent-resistant nanofiltration under low operating pressure, Journal of Membrane Science 501 (2016) 152-160. https://doi.org/10.1016/j.memsci.2015.11.016.

[84] S.L. Aristizábal, L. Upadhyaya, G. Falca, A.Y. Gebreyohannes, M.O. Aijaz, M.R. Karim, S.P. Nunes, Acid-free fabrication of polyaryletherketone membranes, Journal of Membrane Science (2022). https://doi.org/10.1016/j.memsci.2022.120798.
[85] B. Yuan, C. Jiang, P. Li, H. Sun, P. Li, T. Yuan, H. Sun, Q.J. Niu, Ultrathin Polyamide Membrane with Decreased Porosity Designed for Outstanding Water-Softening Performance and Superior Antifouling Properties, ACS Appl Mater Interfaces 10(49) (2018) 43057-43067. https://doi.org/10.1021/acsami.8b15883.
[86] J. Shen, G. Wang, X. You, B. Shi, J. Xue, J. Yuan, Y. Li, J. Guan, Y. Ma, Y. Su, R. Zhang, Z. Jiang, Thermal-facilitated interfacial polymerization toward high-performance polyester desalination membrane, Journal of Materials Chemistry A 9(13) (2021) 8470-8479. https://doi.org/10.1039/d0ta12283a.
[87] B. Liu, S. Wang, P. Zhao, H. Liang, W. Zhang, J. Crittenden, High-performance polyamide thin-film composite nanofiltration membrane: Role of thermal treatment, Applied Surface Science 435 (2018) 415-423. https://doi.org/10.1016/j.apsusc.2017.11.126.
[88] H. Tsai, Y. Ciou, C. Hu, K. Lee, D. Yu, J. Lai, Heat-treatment effect on the morphology and pervaporation performances of asymmetric PAN hollow fiber membranes, Journal of Membrane Science 255(1-2) (2005) 33-47. https://doi.org/10.1016/j.memsci.2004.09.052.
[89] X. Li, Y. Liu, Q. Liu, Z. Zheng, H. Guo, Single-layer membranes for organic solvent nanofiltration: a molecular dynamics simulation and comparative experimental study, RSC Adv 12(12) (2022) 7189-7198. https://doi.org/10.1039/d1ra09061e.
[90] Y. Ma, J.W. Chew, Investigation of membrane fouling phenomenon using molecular dynamics simulations: A review, Journal of Membrane Science 661 (2022). https://doi.org/10.1016/j.memsci.2022.120874.
[91] M. Nilsson, G. Trägårdh, K. Östergren, The influence of pH, salt and temperature on nanofiltration performance, Journal of Membrane Science 312(1-2) (2008) 97-106. https://doi.org/10.1016/j.memsci.2007.12.059.
[92] N.F. Ghazali, N.D.A. Razak, Recovery of saccharides from lignocellulosic hydrolysates using nanofiltration membranes: A review, Food and Bioproducts Processing 126 (2021) 215-233. https://doi.org/10.1016/j.fbp.2021.01.006.
[93] D. Zhao, J.F. Kim, G. Ignacz, P. Pogany, Y.M. Lee, G. Szekely, Bio-Inspired Robust Membranes Nanoengineered from Interpenetrating Polymer Networks of Polybenzimidazole/Polydopamine, ACS Nano 13(1) (2019) 125-133. https://doi.org/10.1021/acsnano.8b04123.
[94] D. Li, R. Wang, T.-S. Chung, Fabrication of lab-scale hollow fiber membrane modules with high packing density, Separation and Purification Technology 40(1) (2004) 15-30. https://doi.org/10.1016/j.seppur.2003.12.019.
[95] G. Székely, J. Bandarra, W. Heggie, B. Sellergren, F.C. Ferreira, Organic solvent nanofiltration: A platform for removal of genotoxins from active pharmaceutical ingredients, Journal of Membrane Science 381(1-2) (2011) 21-33. https://doi.org/10.1016/j.memsci.2011.07.007.